Politecnico di Torino

Politecnico di Torino

Master's Degree in Biomedical Engineering

December 2024

Influence of Microplastic Contaminations on the Barrier Properties of Reconstituted Mucus

Supervisors:

Prof. Gianluca Ciardelli

Prof. Monica Boffito

Prof. Dr Oliver Lieleg

Laboratory tutor:

Fabio Henkel

Candidate:

Angelo Bolano

Summary

Abstract

There is an invisible but inevitable ingredient that is being served on the tables all around the world: microplastics (MPs). Alarmingly, it is estimated that around 5 g of small sized particles (<1mm) are ingested weekly. These particles can accumulate in the gastrointestinal mucosa, which acts as the first biological barrier encountered by MPs up taken with diet. However, it is yet unknown how the presence of such pollutants affects the physiological functionalities of this highly selective barrier. In this study, a microfluidic setup was used to recreate a MPs contamination at the interface of reconstituted gastric mucus (MUC5AC). For this purpose, 300 nm sized differently charged polystyrene nanoparticles were chosen as a model for natural occurring plastic contamination in the sub-micrometer range. This setup allowed to investigate the penetration of differently charged fluorescent test molecules (4 kDa dextrans) into both the reconstituted pristine and contaminated mucin gel. The hydrodynamic radii of these dextrans were at least two orders of magnitude lower than the mesh size of the mucus gel. Hence, the diffusive penetration of the dextrans was modulated by intermolecular interactions rather than geometric hindrance. By means of fluorescence imaging, it was possible to evaluate and compare the penetration profiles of differently charged dextrans into the reconstituted mucus. The obtained results evidenced that the MPs contamination affects the uptake of the selected test molecules at the mucosal interface, suggesting that its barrier properties are affected by the presence of MPs. This study also suggested that alterations in the barrier properties are driven by electrostatic interactions, along with hydrophobic binding of the tested molecules to the contaminating MPs. Overall, the results of this thesis work provide an advancement in the general understanding of how MPs contamination affects the destiny of ingested substances. Furthermore, these findings on the gastric MUC5AC mucin might be reasonably transferred to other mucin types such as the intestinal MUC2. In the long term, these insights may be relevant for drug delivery applications when drugs are intended to overcome a MPs contaminated mucus barrier.

Introduction

In recent years, the pervasive presence of microplastics in the environment has emerged as a significant global concern due to their potential impacts on ecosystems and human health. Microplastics, typically defined as plastic particles less than 5 millimeters in diameter, originate from the intentional production of small particles or the fragmentation of larger plastic items through physical and chemical mechanisms [1], [2], [3]. Intentional production includes microbeads used in personal care products and industrial abrasives. For example, polyethylene and polypropylene microbeads are commonly added to facial cleansers, toothpastes, and exfoliating products to enhance their abrasive properties [4], [5] while fragmentation results from the degradation of plastic waste exposed to environmental factors such as UV radiation and mechanical abrasion. Indeed, a recent study has shown that prolonged exposure to sunlight leads to photodegradation of plastics, breaking them down into smaller particles[6]. At the same time, mechanical forces from natural and anthropic agents lead to the physical abrasion and fragmentation of plastic debris in aquatic and terrestrial environments[7].

These particles are resilient to environmental degradation, leading to their accumulation in terrestrial and aquatic environments.

This widespread distribution of microplastics has facilitated their entry into the food chain through multiple pathways. For example, aquatic organisms often ingest microplastics, mistaking them for food. As these organisms are consumed by predators, microplastics can bioaccumulate and eventually reach humans through the consumption of seafood [8]. Alarmingly, contaminating particles have also been found in drinking water[9] and even table salt[10]. Terrestrial food chains are not exempt: microplastics have been found in agricultural soils due to the application of sewage sludge and plastic mulching films, potentially entering crops and livestock [11]. Additionally, microplastics can contaminate food products through packaging and processing, further increasing human exposure

Given their presence in foods, beverages and cosmetic products, microplastics are very likely to enter the body via the gastrointestinal (GI) tract and interact with the protective mucus layer that lines the gastric epithelium.

The mucus layer is a viscoelastic hydrogel composed of lipids, salts, and, primarily, the mucin glycoproteins [12], [13].

Mucins, the main structural components of mucus, are large, highly glycosylated proteins that form a gel-like network responsible for the mucus's protective and lubricating properties. This gel-like structure allows mucus to trap and immobilize pathogens, particulates, and other foreign materials, preventing them from reaching the epithelial surface[14].

The filtering behavior of mucus is attributed to its porous structure and biochemical properties, which can hinder the penetration of particles above a certain size or with particular surface characteristics[15], [16], [17]. Indeed, mucus filters substances based on size exclusion, allowing only particles smaller than its mesh size of the mucin network to pass through, while larger particles are retained [17], [18], [19]. Additionally, mucus enables filtering based on specific interactions between its components and diffusing substances[20], [21]. Indeed, mucins can interact with a wide range of molecules and nanoparticles through mechanisms such as electrostatic forces, hydrophobic interactions, hydrogen bonding, and disulfide bridge formation[22], [23], [24].

Given these characteristics, nano-sized microplastics may become entrapped within the mucin network of the GI mucus layer, potentially interfering with physiological functions by altering its selective barrier properties. Indeed, these particles might alter the mucus' filtering capabilities by masking existing binding sites or creating new ones. Such alterations could disrupt the mucus' ability to regulate the uptake of substances like nutrients and pharmaceuticals, potentially leading to adverse health effects[25], [26].

Despite these concerns, limited research has been conducted on the interactions between nanoplastics and the GI mucus. The challenges associated with detecting and characterizing nano-sized plastics within biological matrices have hindered progress in this area [27]. This knowledge gap underscores the need for further

studies to elucidate the impact of nanoplastics on mucus barrier properties and to develop strategies for mitigating potential health risks.

To address this knowledge gap, the present study employs a microfluidic approach to establish a reconstituted mucus interface using gastric mucin solutions, purified from porcine stomachs. This method allows for precise control over the experimental environment, enabling investigation of mucus barrier properties under physiologically relevant conditions. Engineered polystyrene nanoparticles (NPs) are selected as a model for nano-sized plastics and introduced at environmentally relevant concentrations to simulate the ingestion of contaminated food substances.

The investigation focuses on how nanoplastics contamination affects the barrier properties of the reconstituted mucus by examining the permeability of molecules with different surface charge characteristics. Specifically, the transport of cationic, anionic, and neutral fluorescent probes across the mucus layer was assessed in the presence and absence of polystyrene NPs. By analyzing changes in diffusion rates and interactions between the NPs and both the mucin network and the test molecules, this study aimed to elucidate the mechanisms by which nanoplastics may alter the selective filtering functions of mucus.

The findings provide critical insights into the potential impact of nanoplastics on gastrointestinal health and contribute to a deeper understanding of how environmental contaminants can affect mucosal barrier properties.

Materials

This study utilized several key components to investigate the influence of nanoplastic contamination on the barrier properties of reconstituted mucus. These primary elements included purified porcine gastric mucin (to model the physiological gastrointestinal mucus), engineered polystyrene nanoparticles (to model nanoplastics) and dextrans as fluorescent probe molecules with varying surface charge characteristics. A microfluidic system was employed to establish a reconstituted mucus layer with a stable sol-gel interface.

1 Reconstituted mucus

Mucus is a viscoelastic secretion that lines various mucosal surfaces throughout the human body, including the gastrointestinal tract, respiratory tract, and urogenital tract [28]. It serves as a crucial protective barrier, safeguarding underlying epithelial tissues from mechanical damage, pathogens, and toxins [14].

One of the key functions of mucus is its selective barrier properties, which regulate the passage of substances based on size and physicochemical interactions. Its barrier properties depend on both size exclusion filtration and interaction filtration mechanisms[20], [26]. It is composed primarily of glycoproteins called mucins, which form a hydrogel network that is mainly responsible for these characteristics[24].

To investigate the influence of microplastics on the barrier properties mucus, this study employed a mucus reconstituted from purified MUC5AC mucins as a model for the physiological mucus.

1.1 Mucins

Along with water, electrolytes, and lipids, mucus is composed of approximately 1%–5% mucin proteins[12]. They consist of a protein backbone rich in serine, threonine and proline residues, which are highly O-glycosylated with oligosaccharide side

chains. These side chains confer a high density of negative charges due to the presence of sialic acid and sulphate groups[28] [12], [22] . These charged domains play a significant role in the mucins' ability to interact with charged molecules through electrostatic interactions [20]. The protein backbone also contains hydrophobic and cysteine-rich terminal regions that mediate mucin-mucin interactions, *i.e*, mucin oligomerization and crosslinking, and, therefore, contribute to the formation of gel networks [29].

Mucins are classified into two main types: membrane-associated mucins and secreted (gel-forming) mucins. Membrane-associated mucins are anchored to the epithelial cell surface and play roles in cell signalling and protection[30], while secreted mucins are released into the mucus layer to form a gel-like matrix that provides mucus with its viscoelastic properties. Several tissue-specific gel-forming mucins play critical roles in different parts of the body. For instance, MUC2 is predominantly expressed in the intestine, MUC5AC is found in the stomach, respiratory epithelium, and cervix, and MUC5B is the dominate mucin species in the respiratory tract and salivary glands.[31], [32], [33], [34]

In this study, a 2% (w/v) MUC5AC solution was utilized. One of the key advantages of handling a MUC5AC solution resides in its ability to undergo acidic gelation, which makes it suitable for the setup employed in this study. Under acidic conditions, MUC5AC forms a gel-like network that resembles the natural mucus barrier found in the stomach.[20], [35]

In this study, MUC5AC was purified in-house from pig stomachs. Lab-purified mucin differs significantly from commercially available ones[23]. Commercial mucins often undergo harsh processing and drying procedures that can degrade their molecular structure and alter their physicochemical properties. In contrast, the in-house purified MUC5AC retains its native conformation and functional characteristics[36], which are crucial for mimicking the natural mucus microstructure. This distinction is important because the structural integrity of mucin polymers influences their gel-forming abilities and interactions with particles such as nanoplastics.

1.1.1 Mucins' gelation mechanism

The mechanism by which MUC5AC undergoes acidic gelation has not yet been totally understood. However, a possible explanation [12] assumes that it involves interactions between amino acids with pKa values around 4, such as Asp and Glu. These are located in the poorly glycosylated terminal regions of mucin backbones. At neutral pH, these regions are organized in random coil configurations, folded together with hydrophobic domains [37]. These folded structures are likely stabilized by salt bridges existing between Asp and Glu. At pH ≤ 4, the carboxylate groups of these amino acids protonate, breaking those salt bridges that held together the folded structure, resulting in the unfolding of the random coils to elongated, rod-like structures. This conformational change exposes the hydrophobic domains that were hidden in the folded structures [12], [37]. The hydrophobic interaction of these domains act as crosslinks between adjacent mucin proteins, resulting in the formation of a viscoelastic hydrogel network.

2 Polystyrene nanoparticles

While the term "microplastics" encompasses a broad range of particle sizes and shapes, there is increasing attention on the smaller fraction (<1 μm) also defined as nano-sized plastics [38]. Nano-sized plastics are of particular concern due to their small size, which could allow them to cross biological barriers such as mucus and interact with cellular components, potentially leading to toxicological effects [39]. Moreover, their high surface area-to-volume ratio likely increases their reactivity and ability to absorb and transport pollutants, potentially leading to their harmful accumulation at the level of the mucosal barriers.

Despite their potential health risks, nanoplastics remains the least studied category of microplastics. Therefore, to gain insights on this topic, this study focused on the potential adverse effects of this minute class of plastic contaminants.

However, the vast variety of shapes and chemical compositions of different environmentally occurring nanoplastics poses an experimental challenge because their heterogeneity adversely affects the reproducibility of experimental results. Hence, to study the mechanistic principles governing the interactions of microplastics with mucosal interfaces, here, this heterogeneity is eliminated by choosing engineered polystyrene nanoparticles (NPs) (Magsphere Inc.1993 E. Locust Street Pasadena) with a nominal diameter of 0.3 μm as a simplified model system for real-world nanoplastic. Moreover, to account for their diversity of surface properties, two variants differing in surface charge were employed: aminated cationic NPs and carboxylated (AMF-300NM) anionic NPs (CAF-300NM). In addition, the NPs were fluorescently labeled so that they could be traced under fluorescent microscopy.

2.1 Selecting an environmental relevant nanoparticles' concentration

Quantifying the concentration of nanoplastics in environmental and biological samples is a complex quest due to limitations in detection methods and the heterogeneous nature of plastic pollution [27]. The presence of micro- and nanoplastics varies significantly depending on the sample analyzed, influenced by factors such as geographical location, sampling techniques, and environmental conditions [40]. Studies have reported a wide range of microplastic concentrations in a wide variety of environmental and edible products samples, with levels often fluctuating by several orders of magnitude [11], [41], [42]. Indeed, while some studies detected tens to hundreds of microparticles per kg of table salt [43] and seafood [44], others have found particles in the range of several millions per kg of

sample, released in food by items such as food containers [45], baby feeders [46] and plastic teabags [47]. Alarmingly, a study on toothpastes and facial cleansers found them at concentrations up to 1%, the equivalent of billions of particles per milliliter of product [4], [48]. However, the lower detectable size in these studies was often over the threshold of 1 µm, meaning that a void in the quantification of nano-sized particles is left.

Unfortunately, precise data on those smaller sized plastic particles (<1 µm) is limited. In fact, they are particularly difficult to detect and analyze at environmental concentrations and in biological matrices [49]. Their small sizes pose substantial difficulties in separation, visualization, and chemical identification. Thus, they are more challenging to quantify with current analytical techniques, potentially leading to an underestimation of their abundance in food and beverages. Indeed, their smaller size enhances their ability to penetrate food systems and accumulate over time, suggesting that the concentrations of the nano-sized particles may be significantly higher than those detected by far, of the larger ones.

Considering this scenario, in this study, a concentration of 0.05% w/v (~10^{12} particles/ mL) was selected to resemble an environmentally plausible level of nanoplastic contamination in ingested materials.

3 Dextrans

Dextrans are biologically inert polysaccharides there previously used in studies of biological barriers permeability [20], [21], [53], [54]. They are available with a variety of grafted molecules, allowing to tune chemical properties such as, i.e., fluorescence and charge. Here, as molecular platform to study the barrier properties of mucin gels, fluorescein isothiocyanate (FITC)-labeled dextrans with a molecular weight of ~ 4 kDa were chosen. Three variants exposing different charges were used: unmodified, diethylaminoethyl (DEAE)-grafted, carboxymethyl (CM)-grafted-dextrans.

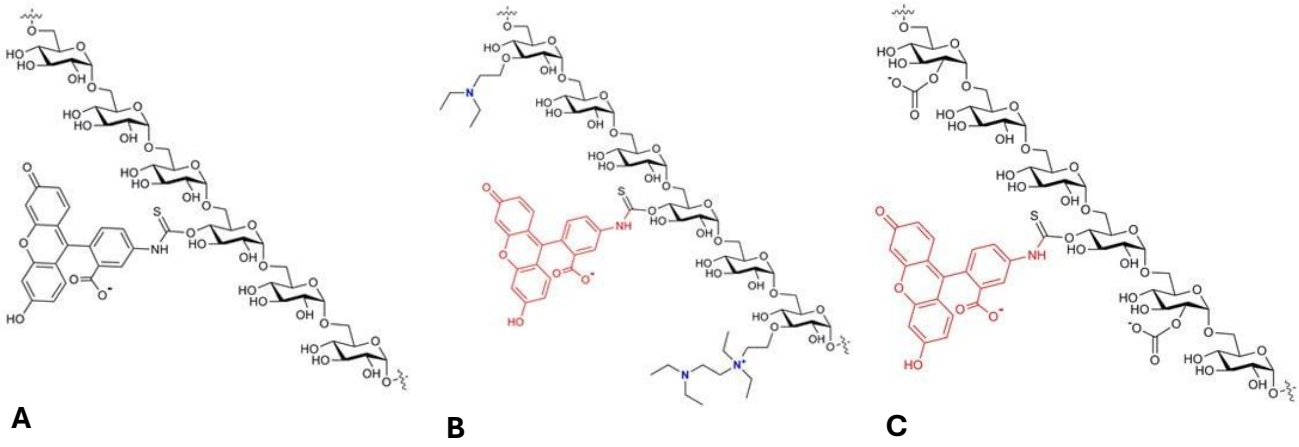

Figure 1 *Structure of dextrans*. Schematic illustration of the chemical structure of unmodified dextran (close to electrostatically neutral) (A), DEAE-modified (cationic) dextran (B) and CM-modified (anionic) dextran (C). All dextrans carry a FITC fluorescent label. Images taken from Merck KGaA website

Dextrans were chosen as test molecules because their controlled molecular weight allows for the assessment of permeability based on molecular interactions rather than size differences, providing a consistent basis for comparison. Moreover, the variability in surface charge among the selected dextrans enables the investigation of how electrostatic interactions influence diffusion through the mucus layer. The fluorescent labeling of dextrans enables tracking of their diffusion using fluorescence microscopy, allowing evaluation of transport across the mucus barrier. Moreover, dextrans are biocompatible and do not interfere with the structural integrity of mucus, making them ideal for in vitro studies where preserving the native properties of mucus is essential. The fact, that similar dextrans have been used in previous studies[20], [21] enables comparability of the results found throughout this study with those reported in literature.

4 Microfluidic setup

To study the barrier function of mucus effectively, it was essential to establish a well-defined mucus interface. Microfluidic devices offer precise control over fluid flow and microenvironmental conditions, making them suitable for creating such an interface. In this study, a microfluidic-chip was employed to reconstitute the mucus layer enabling the establishment of a stable sol-gel interface. Its geometry, showed (Fig 2) was previously designed Marczyski *et al.*[20]

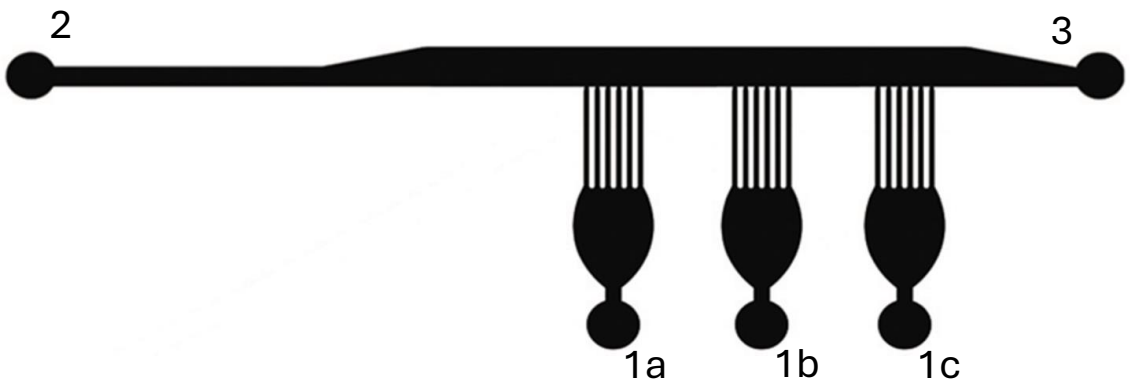

Figure 2 *Microfluidic geometry.* Schematic illustration of the microfluidic geometry showing the mucin reservoirs ("hand-like" structures) with the inlets (1a, 1b, 1c) and buffer channel (horizontal channel) and its inlet and outlet holes (2,3)

In this geometry, three "hand-like" channels serve as mucus reservoirs. The mucin solutions are loaded through the lower inlets, filling the vertical "finger-like structures until the intersection with the horizontal channel that serves as buffer reservoir. At the intersection of the vertical and the horizontal buffer channel, a stable reconstituted mucus interface is then established by inducing acidic mucin gelation *in situ*. Moreover, by subsequently flushing NPs-contaminated buffers and

test molecules solutions, it is possible to image the system and evaluate the effects of the NPs contaminations against the barrier properties of such interface.

Methods

If not stated differently all chemicals were purchased from Carl Roth (Karlsruhe, Germany).

1 Mucin purification

Porcine gastric mucin MUC5AC was purified manually as previously described by Marczynski *et al*[21].

Fresh porcine stomachs were purchased from a local butcher (Mundlhof, Allershausen, Germany), cut open and gently rinsed to wash away their food content. The raw mucus was then collected by manually scraping the inner wall of the stomachs. The collected mucus was diluted 5-fold in 10 mM sodium phosphate buffer (pH 7.0) containing 170 mM sodium chloride to shield electrostatic interactions between the mucin molecules and potential impurities attached to them. Additionally, 0.01% sodium azide was added to the raw mucus solution, which was stirred at 4 °C overnight for homogenization. Sodium azideNaN_3 is a well know bacterial and fungal growth inhibitor: here, it was added to avoid bacterial degradation of the mucin. Coarse impurities and cellular debris were removed by ultracentrifugation (150 000 g for 1 h at 4 °C). To separate mucins from other macromolecules, the supernatant was collected and purified by size exclusion chromatography using an ÄKTA purifier system (GE Healthcare, Germany) and an XK50/100 column packed with Sepharose 6FF resin (stationary phase). Here, the suspended macromolecules are separated according to their molecular volume. Thus, when crossing the column, the molecules interact with its porosities. The smaller the size of the molecules the higher the number of interactions with the stationary phase. This effect results in a direct proportionality between the molecular volume and velocity, allowing to separate the molecules according to the

time (elution time) they need to cross the column. By calibrating the instrument, it is possible to associate the elution time to the molecular weight.

In the next step, cross-flow filtration (Cytiva, hollow fiber cartridge, 300 kDa molecular weight cut-off (MWCO), Marlborough, USA) was employed to desalt the obtained mucin solution using cross-flow filtration using a membrane with a molecular cut-off of 100 kDa. The purified mucin solution was then lyophilized and stored at -80 °C.

2 Rheological measurements

The viscoelastic properties of the reconstituted mucin gel were previously tested by the lab technician Tobias Fuhrman as part of the general quality assessment of the purified mucins. To conduct the measurements, 1 mL of 2% w/v mucin gel was prepared. First, 900 µl of ultrapure water were added to the lyophilized mucin and incubated a room temperature on a rolling shaker for 1h to allow complete dissolution. Then, to induce acidic gelation, 100 µl of 100 mM sodium acetate buffer (pH 4.0) were added to the solution.

The rheological characterization has been performed with a research grade shear rheometer (MCR 302, Anton Paar, Graz, Austria) equipped with a plate-plate geometry (P-PTD 200/AIR, Anton Paar bottom plate; PP25 25 mm Anton Paar steel measuring head). All experiments were conducted at constant temperature T=20 °C, with a plate separation gap of 0.3 mm and a sample volume of 250 µL.

During the rheological measurements the linear viscoelastic (LVE) region of the material response must not be exceeded, because the LVE region indicates the strain range that ensures a non-destructive deformation of the sample [50]. Hence, for each sample a pre-test was performed to ensure that throughout all subsequent rheological measurements LVE regime is not exceeded. During the pre-test a minimum applicable torque was applied to the sample, while monitoring the

resulting strain of the sample. This strain was multiplied by a factor of 1.5 and used as a target strain for the following rheological measurements.

Subsequently, a frequency sweep test was performed. Here, the storage modulus (*G'*) and the loss modulus (*G''*) were measured over a frequency range from 0.1 Hz to 10 Hz in a strain-controlled mode using the previously determined target-strain

3 Surface potential measurements

To understand the physical principles underlying surface potential measurements, it is essential to consider the electric double layer (EDL) phenomenon. This occurs when a solid surface is immersed in an electrolyte solution, leading to interactions between the ions in the solution and the surface due to electrostatic forces. The EDL consists of two distinct layers:

- Stern layer: a tightly bound layer of counterions (ions with an opposite charge to the surface) adheres strongly to the surface, forming a stationary layer.
- Diffusive layer: surrounding the stern layer causes the formation of a loosely bound layer of ions. Unlike the Stern layer, the ions of this layer are not fixed and are continuously exchanged with free ions in the electrolyte solution.

The charge distribution at a solid-liquid interface generates an electric potential between the surface and the adjacent solution. This potential gradually diminishes with increasing distance from the surface. The potential at the outer boundary of the Stern layer, also referred to as the slipping plane, is specifically defined as the zeta potential.

Zeta potential is an important interfacial property because it reflects not only the surface charge but also the characteristics of the surrounding solution, such as ionic strength and pH.

To evaluate the zeta potential of a surface, several techniques can be employed, depending, i.e. on the geometry of the sample to be tested. In this study, streaming potential and electrophoretic light scattering measurements were performed.
While electrophoretic light scattering was employed to measure the zeta potential of both the NPs and the dextrans, the streaming potential measurement was employed to evaluate the surface potential of a mucin monolayer, which was intended to resemble the interface of a mucus.

3.1 Streaming potential

Streaming potential measurements are employed to evaluate the zeta potential of flat surfaces. The measurement is based on the mobilization of the ions of the diffusive layer due to relative motion of the surface and the solution. Briefly, in the measuring chamber, two sample foils are moved close, so that the coated surfaces are parallel to each other. A small gap is left (approx. 100 µm), resulting in the formation of a capillary channel. When the measuring solution is flushed in the capillary, the EDL forms. Then, a pressure gradient streams the solution through the capillary, dragging the ions of the diffusive layer to the downstream end of the samples. This redistribution of ions causes a difference in the charge distribution on the sample's surface. These phenomena result in the generation of an electrical potential that is registered by the electrodes that are placed at the at the upstream and downstream ends of the samples.

Since the zeta potential of the mucus interface is an important parameter governing its barrier properties, its value was evaluated with streaming potential measurements in both pristine and NPs-contaminated conditions. These measurements were performed on a mucin monolayer that was intended to resemble the interface of the reconstituted mucus, To do so, first, the mucin monolayer was created as described in the following chapter.

3.1.1 Creation of mucin monolayer

In order to evaluate the effects of NPs contamination on the zeta potential of the mucus surface, this was modeled by creating a mucin monolayer on a thin foil. To do so, the protocol established by Rickert *et al*. [51] was followed as described below.

The monolayer of mucin was grafted on a thin foil (thickness of approx. 150 – 200 µm) of a polycarbonate-based, thermoplastic, aromatic polyurethane (PCU) material (Carbothane AC-4085A, Lubrizol Advanced Materials, USA) via a carbodiimide-based process as described in the following. Then, the monolayer was either contaminated by a NPs solution or left as such and the surface zeta potential was measured with a SurPASS 3 Eco device (Anton Paar) equipped with an adjustable gap measuring cell for planar samples (Cat.No. 159 880, Anton Paar). The details of this experiment are as also described in the following paragraphs.To measure the zeta potential of a mucin gel surface First, the PCU surface was activated in atmospheric plasma at 56 W for 25 min at 0.4 mbar (plasma oven: SmartPlasma 2.0, plasma technology GmbH, Herrenberg, Germany). This process oxidizes the PCU's surface, creating reactive hydroxy groups that will allow the following grafting process. Next, N [3 Trimethoxysilyl)propyl]ethylenediamine triacetic acid trisodium salt (TMS-EDTA) (abcr, Karlsruhe, Germany) was dissolved in 10 mM sodium acetate (pH = 4.5) at a ratio of 0.1% (w/v). TMS-EDTA carries, on one end, a silane group that is used to couple the molecule to the surface. On the other end, it exposes a carboxyl groups that can react with the amino residues on the mucin protein to form a covalent bond. To do so, the carboxyl groups of the silanes were activated: the PCU foil was incubated at room temperature (RT) inside a petri dish for 30 min with 10 mL of 2-(N-morpholino ethanesulfonic acid buffer (MES, AppliChem GmbH,Darmstadt, Germany, pH 5.0) containing 5 mM 1-ethyl-3-(3-dimethylaminopropyl)-carbodiimid-hydrochlorid (EDC) and 5 mM N-Hydroxysulfosuccinimide (sulfo-NHS). This solution was prepared just before the incubation to avoid hydrolysis of the coupling molecules.

Next, the EDC-NHS solution was replaced with Dulbecco's phosphate buffered saline (DPBS, pH 7.4, Sigma-Aldrich Inc., Darmstadt, Germany) containing 0.1 % (w/v) of the purified mucin. Overnight incubation at 7 °C on a tilting plate followed. The low temperature during this step reduced the risk of mucin degradation and the gentle agitation allowed to establish an homogenious coating. Finally, the coated foils were retrieved from the mucin solution and loosely adsorbed mucins were rinsed away by dipping the foils in 80 % ethanol. The coated PCU was then stored in DPBS at 4 °C until further use.

Before further use, the coated foils were equilibrated in 10 mM sodium acetate buffer (SA) at pH 4 for 10 min. This step was important since the protonation degree of the mucin's residues is dependent on pH. Thus, the electrostatic interaction with the NPs might change when changing the pH. To create microplastic contaminations on the mucin coatings, the sodium acetate buffer was replaced by a 10 mM sodium acetate buffer containing 0.05% (w/v) of either anionic or cationic polystyrene NPs. After 30 min incubation at RT on a tilting plate, the foils were dipped into the pristine SA buffer to rinse away the loosely bound NPs.

3.1.2 Streaming potential measurement

For the streaming potential experiment, the pristine and the contaminated mucin coated PCU foils were cut into rectangles with a scalpel and attached to a flat sample holder using double sided tape. Next, the sample holder was placed into an adjustable gap measuring cell (Anton-Paar), which was mounted to the streaming potential measuring device (Surpas, Eco, Anton-Paar). The following four groups of PCU foils were measured using an aqueous 1 mM potassium chloride solution at pH 4.0 as an electrolyte solution: uncoated, mucin coated, mucin coated with cationic NPs contamination, mucin coated with anionic NPs contamination. For each group, a minimum of three streaming potential measurements was performed.

3.2 Electrophoretic light scattering

Electrophoretic light scattering (ELS) applies a constant electric field to a sample solution containing charged particles. The charged particles migrate toward the electrode with the opposite charge, a phenomenon referred to as electrophoretic mobility. The velocity of this movement is directly proportional to the particle's surface charge, which is influenced by the surrounding medium and the particle's zeta potential.

To measure zeta potential, ELS utilizes a laser to illuminate the moving particles. As the particles scatter the laser, their motion induces a Doppler frequency shift in the scattered light. This frequency shift is directly related to the velocity of the particles. By analyzing the time-dependent variations in scattered light intensity using autocorrelation functions, the system calculates the electrophoretic mobility of the particles, from which the zeta potential can be derived.

The relationship between electrophoretic mobility (u) and the zeta potential (ζ) is given by the Helmholtz-Smoluchowski equation:

$$u = \frac{\varepsilon\zeta}{\eta}$$

- u: Electrophoretic mobility [m2/Vs]
- ε: Dielectric constant of the solvent [F/m]
- ζ: Zeta potential [V]
- η: Viscosity of the solvent [Pa·s]

This equation establishes that zeta potential is proportional to the electrophoretic mobility, considering the solvent’s properties.

3.2.1 Nanoparticles' zeta potential evaluation

The zeta potential of the polystyrene NPs was measured *via* ELS using a Litesizer500 Zetasizer (Anton-Paar, Graz, Austria). For these experiments, 1 mL of a 20X diluted low molarity contaminated buffer was loaded into the measurement cell (Omega cuvette) and analyzed at RT.
To ensure data reproducibility, at least three measurements were conducted for both the anionic and the cationic NPs.

3.2.2 Test molecules' zeta potential evaluation

To measure the charge of the test molecules, each dextran variant was dissolved in 5 mM sodium acetate buffer (pH = 4.0). Then, the samples were bleached under a common table lamp for 30 minutes to avoid interference of their fluorescence with the scattered light registered by the device's sensors. This step was meant to obtain more accurate results. Then, each solution was loaded in the measuring cell of the Litesizer500 and ELS measurement was performed. Three repetitions per group were conducted to ensure experimental consistency.

4 Evaluation of dextrans' attachment to nanoparticles

The attachment of the unmodified dextrans to the aminated NPs was evaluated with two methods. One evaluated the shielding of the NPs' surface potential cause by the attachment of dextrans, while the other evaluated the attachment of dextrans by registering their fluorescence.

4.1 Zeta potential shielding effect evaluation

Dextrans attachment to NP was investigated by evaluating their shielding effect on the NP's zeta potential. Briefly, 0.5% w/v unmodified dextrans were added to 5 mM sodium acetate buffer (pH 4) containing 0.05% w/v NPs, and incubated for 20 min. Then, the particles were washed 3 times (5 min centrifugation at 7500 rcf followed by supernatant replacement with clean buffer). Finally, the solution was diluted 20 times in 5 mM sodium acetate buffer and analyzed *via* ELS technique.

4.2 Fluorescence of attached dextrans

Here, dextrans were dissolved in different salts with the purpose of hindering dextrans attachment to the nanoparticles. Aminated NPs were immobilized on the surface of a polystyrene 96 well-plate, then incubated with the dextrans
The wells' surface was treated to expose a silane layer that carried carboxyl groups. These would react with the amino groups present on the NP surface, resulting in a peptide bond that led to immobilization of the NPs on the wells' surface.
Precisely, the plate was first treated with air plasma at 30 W for 90 s at 0.4 mbar. This process created hydroxyl groups, that would enable the covalent attachment of the silanes to the wells' surface. Add ref
To form the covalently bound silane layer, TMS-EDTA was dissolved in 10 mM sodium acetate (pH = 4.5) at a ratio of 0.1% w/v. TMS-EDTA carries a silane group and, on the other end, the 3 carboxyl groups that will react with the amino groups of the NP. Then, each well was incubated with 100 µL of the solution at 60°C for 5 h to induce the formation of the covalent bonds. Subsequent incubation at 40 °C for 8.5 h stabilized the bonds. Then, the wells were washed 3 times with 80% ethanol and let dry at room temperature for 1 h.
In the next step, the carboxyl groups of the silanes were activated. Here, the wells were incubated at room temperature for 30 min with 100 µL each of buffer MES (pH

5.0) containing 5 mM EDC and 5 mM sulfo-NHS. This solution was prepared just before the incubation to avoid hydrolysis of the coupling molecules. After the incubation, the EDC-NHS solution was replaced by DPBS (pH 7.4) containing 0.05% (w/v) aminated NPs. A blank group was also prepared by skipping the addition of NPs to the last solution. The well-plate was incubated at RT on a tilting plate, to allow an even coating of the wells' surfaces. Eventually, the wells were washed 3 times with 10 mM acetate buffer (pH 4.0).

Four dextran solutions containing different compunds were prepared. Unmodified dextrans were dissolved in 10 mM sodium acetate buffer (pH = 4.0) as itself and with the addition of, separately, 5 M guanidine chloride phosphate, 5 M urea and 5 M sodium chloride. The pH was adjusted to pH = 4.0. 100 µL of each solution was separately added to the NP coated wells and incubated for 20 min. Then, the wells were rinsed 3 times with sodium acetate buffer to eliminate the dextran molecules that didn't attach to the NP.

A plate reader (Varioscan Lux, Thermo Fisher Scientific, Waltham, USA) was used to register the fluorescent signal from the NPs immobilized on the well plate, prior to the incubation with the dextrans (excitation 530 nm, emission 578 nm), and the the fluorescent signal emitted by the attached dextrans (excitation 495 nm, emission 520 nm).

As a normalization step, the dextrans' signal from each well was divided by the NPs signal from the same well. The blank's value was calculated as the mean of the signal () from the uncoated wells and subtracted from the signal emitted by dextrans (~ 520 nm)

4.3 Statistical analysis

Unless stated otherwise, all statistical analyses were conducted using Origin(Pro) (Version 2022, OriginLab Corporation, Northampton, USA). Initially, a Shapiro-Wilk test was utilized to determine if the data in the sample groups were normally distributed. Following this, homoscedasticity among the groups was assessed

using Levene's test implemented in Matlab (R2021, MathWorks, Natick, USA). Depending on the results of these preliminary tests, an appropriate two-sample test was selected to evaluate statistically significant differences between the sample groups, with a significance level set at $p < 0.05$. If the data exhibited normal distribution and equal variances (homoscedasticity), a parametric t-test was performed; in cases of unequal variances (heteroscedasticity), Welch's correction was applied to the t-test. If the assumption of normality was not met, a non-parametric Mann-Whitney test was employed as an alternative.

5 Size measurements

5.1 Dinamic light scattering

Dynamic light scattering (DLS) technique analyses suspended particles' size by measuring the fluctuations in light intensity scattered by those particles undergoing Brownian motion. A laser beam is directed through the sample, and when it encounters the suspended particles, the light is scattered in all directions. The scattered signal is captured by the instrument's detectors, which record its intensity over time.

As the particles move randomly in solution, their positions change continuously. These positional changes alter the scattered light's intensity in a time-dependent manner. This variation is analysed using autocorrelation functions to determine the translational diffusion coefficient (*D*).

The hydrodynamic radius of the particles is then calculated from *D* using the Stokes-Einstein equation:

$$D = \frac{k_B\, T}{6\pi\, \eta\, R_H}$$

- D: Translational diffusion coefficient [m^2/s]
- k_B: Boltzmann constant [$m^2 \cdot kg/K \cdot s^2$]
- T: Absolute temperature [K]
- η: Solvent viscosity [Pa·s]
- R_H: Hydrodynamic radius [m]

In this equation, D is inversely proportional to R_H, allowing the particle size to be determined from the measured diffusion coefficient and the known experimental conditions. By correlating the time-resolved intensity fluctuations with the particle motion, DLS provides precise measurements of particle size in the nanometer range.

5.1.2 Data acquisition

The hydrodynamic radii (R_H) of NPs were measured with DLS on the Litesizer 500. The measurement was conducted at room temperature (25 °C) using a 1 mL sample of 5 mM sodium acetate buffer (pH 4) containing 0.05% w/v NPs diluted 20 times, pipetted into a disposable four clear sided measuring cuvette.

6 Microfluidics

The microfluidic devices used in this study were fabricated as previously described by Marczyski et Al. [20]. Briefly, highly transparent devices were obtained by combining glass slides to an elastomeric polymer constructs obtained by soft lithography.

6.1 Masters preparation

The molds (masters) were produced by soft-photolitography on silicon wafers (Siegert Wafer, Aachen, Germany).

For that purpose, a thin layer (approximately 100 µm) of negative photoresist (EpiCore, micro resist technology, Berlin, Germany) was spincoatedspin coated onto a 3 inches silicon wafer (15s at 300 rpm to spread the resin, then 30s at 1000rpm to reach the desired thickness). To partially stabilize the resin, a precuring step was performed by incubating the coated wafer on a hot plate (5min at 65°C, then 10min at 95°C). After cooling to room temperature, the photomask that comprises UV transparent regions defining the desired channel geometry was placed over the photoresist layer. Then, it was radiated with UV light (M365L2, Thorlabs, Newton, USA, wavelength: 365 nm) to induce the resin cross-linking. Post exposure curing (5min at 65°C then 20min at 95°C) was undertaken to stabilize the cross-linked resin. Next, the microfluidic master was developed by dissolving the non-exposed regions of the photoresist layer to reveal the desired channel geometry. For that purpose, the cooled wafer was immersed in an organic solvent (mr-Dev 600, Micro resist technology) for 15 minutes. Finally, the developed wafer was rinsed with fresh developing solution and isopropanol to completely remove the developer.

6.2 Silicone casting and chip assembly

Microfluidic chips were cast from the previously prepared microfluidic masters comprising the negative structure of the desired channel geometry. In detail liquid Polydimethylsiloxane (PDMS) (Sylard 184, Dow Corning, Midland, MI, USA) prepolymer was mixed in a 10:1 ratio with a corresponding curing agent (Dow Corning Sylgard 184, Midland, MI, USA). It was degassed in a vacuum chamber for 30 min to eliminate air bubbles that would compromise the channel geometry and

the device's transparency. The mixture was then poured onto the previously prepared masters inside a petri dish and again degassed for 30 min. The petri dish was dried at 70 °C for 1 h to induce the polymerization of PDMS. Subsequently, the cured PDMS was peeled off from the master and cut into single chips. Inlets and outlets were punctured using a biopsy punch. In the next step, the microfluidic devices were assembled by covalently bonding the PDMS to common microscopic glass slides. To do so, the surface of both were exposed to air plasma (30 W, 30 s, 0.4 bar), then immediately attached to each other by applying gentle pressure. Finally, the microfluidic chips were cured at 70°C for 8h, to restore the original hydrophobicity of the PDMS, which is lost during the plasma activation. This process resulted in an irreversible bond between the glass and the PDMS constructs such that the two surfaces could not be separated without disrupting the bulk structure of PDMS. In the obtained device the channels resulted sealed, so that no liquid could leak from the channels.

6.2.1 Plasma treatment effect

To understand the mechanism by which the PDMS and the glass surfaces form an irreversible bond, the surfaces chemistry and the effect of plasma treatment on the abundance of the exposed functional groups must be analyzed.

Glass is formed by silicate tetrahedron chains, where some oxygen atoms act as bridges between silicon atoms (Si-O-Si) while others don't, resulting in the formation of hydroxyl groups (Si-OH). On the other side, PDMS chains are formed by the repetition of $-OSi(CH_3)_2O-$ units.

During the plasma treatment, the methyl groups on the PDMS surface are oxidized into hydroxyl groups [52]. When put in close contact, the hydroxyl groups on the PDMS surface condensate with the hydroxyl groups on the glass surface, forming a covalent silane bond Si-O-Si [53] responsible for the irreversible binding of the surfaces. Moreover, the formation of hydroxyl groups on the PDMS is responsible for

the loss of its surface's hydrophobicity. In this protocol, it was regained with the last curing step.

Regarding the glass, it was found that the plasma treatment reduces the quantity of hydroxyl groups on its surface[53]. Since the strength of the bond with the PDMS directly depends on their abundance, the plasma treatment should be counterproductive. However, plasma also produces a cleaning effect, reducing the amount of organic contamination at the surface[54]. Thus, cleaner surfaces result in better contact, therefore in a stronger bonding.

6.3 Establishing a sol-gel interface in the microfluidic chip

Once the microfluidic device was fully assembled, the next step was aimed at obtaining a mucin sol/gel interface in the microfluidic system. To do so, first, mucins were dissolved on a rolling shaker for 1 h at a ratio of 2% (w/v) in ultrapure water. Then, the mucin reservoirs of the microfluidic chip (se Fig 2) were filled with approximately 2 µL of the mucin solution under an inverse microscope. After the solution had reached the end of the columns, the inlets to the reservoirs were closed with a droplet of candle wax. Subsequently, 10 µL of 10 mM sodium acetate buffer (pH 4.0) were gently flushed in the main channel to induce acidic *in-situ* gelation of the mucin solution. After 10 min of incubation, the mucin solution was considered to be in a gel state.

6.4 Contaminating the interface

To contaminate the mucin's interface, 10 µL of 10 mM sodium buffer (pH 4) solution containing either cationic or anionic NPs were flushed into the main channel of the microfluidic system. This step allowed interactions between the nanoparticles and the mucin interface. The incubation time was set to 30 minutes, a duration selected based on two important considerations. First, empirical observations during the

development of the microfluidic setup demonstrated that extending the incubation time beyond 30 minutes resulted in destabilization of the gel interface. This instability could compromise the integrity of the interface and affect the reliability of subsequent experimental steps. Secondly, the chosen incubation time had to align with the timing of the natural gastric emptying process. Coherently, on average, approximately 70% of the initial gastric content remains in the stomach after 30 minutes [55]. Hence, the chosen incubation time is in the range of the physiological period during which food remains in contact with the gastric mucosa

Following the incubation, 10 µL of pristine sodium acetate buffer was used to rinse the channel. This flushing step removed the NPs-contaminated solution, ensuring that only nanoparticles that adhered to the reconstituted mucus surface remained in the channel.

To qualitatively observe the presence of nanoparticles at the interface, fluorescent and images were taken with 10x/0.25 Leica objective on the inverted microscope Leica DMi8 (Leica, Wetzlar, Germany) using a digital camera (Orca Flash 4.0 C11440-22C, Hamamtsu, Japan) and the software Leica Application Suite X (version 3.0.4.16529, Leica). For the fluorescent images, a TXR red light filter was used to shine the nanoparticles with an excitation wavelength of 540-580 nm.

6.5 Molecular penetration assay

The core of this study consisted in tracking the penetration of charged molecules across the reconstituted mucin gel. In particular, the penetration behaviors, through the pristine and the contaminated mucus gel, of three variants of fluorescent dextrans were separately evaluated.

For this purpose, the previously established mucin-gel interface with and without microplastic contamination was exposed to the differently charged test molecules.

To do so, each dextran variant was added to 10 mM sodium acetate buffer (pH 4) at a ratio of 0.5% w/v and shortly vortexed to ensure homogeneous suspension of the dextrans. The selected dextran solution was flushed in the microfluidic chip through the right hole of the buffer channel. This step directly followed the surface contamination step (Chapter 5.4). For the control groups on pristine reconstituted mucus, the contamination step was skipped and the dextran solution was flushed in directly after the formation of the mucin gel (Chapter 5.3).

Fluorescent images of the finger like structures were captured after 20 minutes with the inverted microscope Leica DMi8 and an 4x objective (4x/0.10, Leica) objective and a FITC green filter set for the excitation and emission light.

6.6 Data analysis

To quantify the fluorescent signal emitted by the dextrans during the molecular penetration assay, each "finger-like" channel was isolated and analyzed separately using Photoshop (Adobe Inc., 2023) and Matlab (MathWorks, 2023)

A rectangle of 22 pixels in width and 550 pixels in height was chosen as region of interest (ROI) and positioned on each microchannel so that the upper 100 pixels were located on the buffer channel. The fluorescence intensity of the first 50 pixels of this upper region we averaged and set as refence value for the concentration of the dextran solution (0.5% w/v). Then, the pixels of the remaining part of the ROI were averaged line per line, obtaining a vector of 500 pixels, where each pixel represented the average intensity at a certain depth of that specific finger-like structure. Each pixel of the vector was then normalized to the refence value previously calculated. This normalization step was necessary to compensate photobleaching effects during the measurement and differences in fluorescent intensity between the different dextran variants.

The intensity vectors of at least 25 finger-like structures per group were averaged resulting in a single vector**.** Its values were then plotted against the depth of the channel, where the value 0 was associated to the level of the gel interface.

Results and Discussion

1 Modeling microplastic contaminations of mucosal surfaces

1.1 Modeling nanoplastics

Previous studies showed that the permeability of particles with sub-micrometer dimensions through mucins solutions depends strongly on their hydrodynamic diameter [56]. This is because mucin hydrogels are composed of a polymeric network that that prevents the entry of particles bigger than the mesh size of the polymeric network.
Analysis of the size of the polystyrene nanoparticles shown in Fig. 3a show that the aminated and the carboxylated particles have similar hydrodynamic diameters of about 300 nm. The mesh size of gastrointestinal mucus has been reported to range up to 500 nm[57]. Hence, based on their dimension, the nanoparticles used in this study should be able, be able to diffusively enter the mucin network.

Aside from size, it has been demonstrated that, an acidic mucin hydrogel, can interact with charged particles of both algebraic signs via coulomb forces. Hence the mucin network acts as an electrostatic filter that is able to immobilize charged particles even if they are smaller than the mesh size of the mucin network [35]. This is because, the interaction of particles and mucus is not only driven by geometrical hindrance, but also by the electrostatic interactions with the charged domains on the mucin proteins. This information is particularly relevant when choosing a model for NPs contaminants. Indeed, several studies affirm that microplastics found in the environment can absorb chemical compounds on their surface, thereby altering their surface potential [58], [59], [60], [61], [62]. To investigate how differently charge

microplastic contaminations affect the barrier properties of mucin networks, two types of NPs are used to consider this variability.

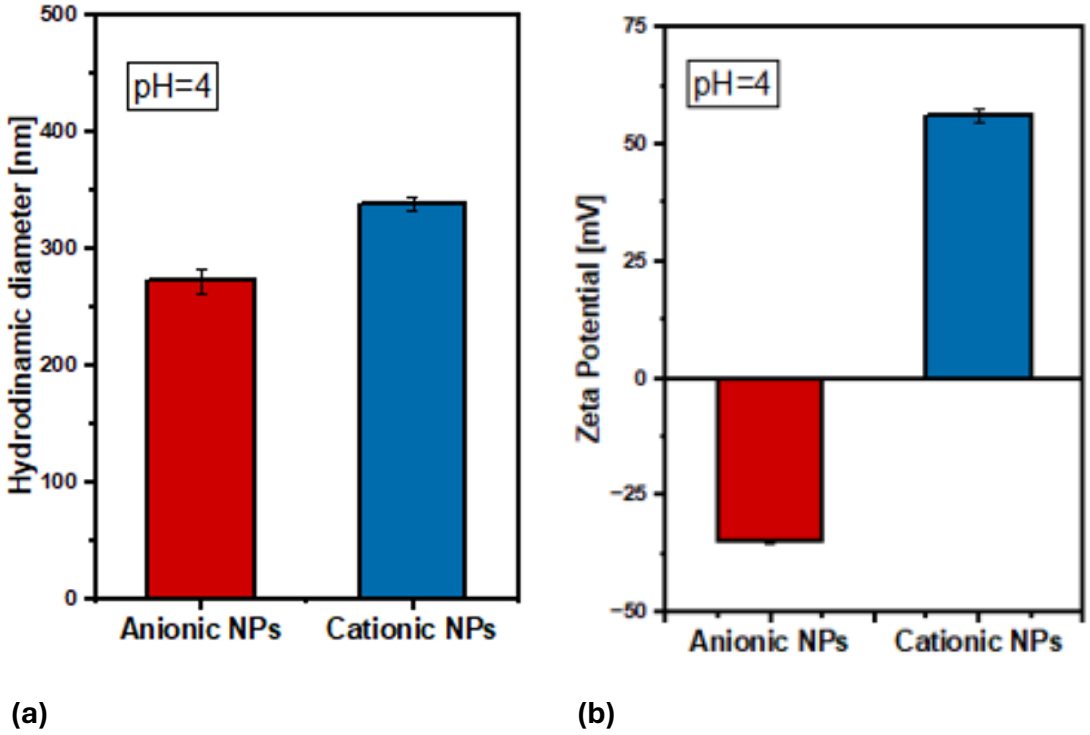

Figure 3 *Polystyrene nanoparticles' characterization*. Plots showing the hydrodynamic size (a) and surface potential (b) of the NPs used to model microplastics
n=3, error bar= SEM

Positively polystyrene NPs modified with amino groups grafted on their surface are used to model cationic nanoplastics. Even though the pK value of these groups depends on their molecular surrounding, most of these groups are protonated in acidic conditions, therefore exposing a positive charge. Hence, the resulting zeta potential of the aminated particles's surface should be positive. Indeed, the data shown in (Fig. 3.b) confirms this assumption, assessing their positive zeta potential. Instead, the groups on the carboxyolated NPs are expected to be not fully protonated, therefore still exposing a negative charge. Again, the registered data indicates a negative zeta potential, confirming the expectations.

1.1 Charged nanoparticles contaminations modify mucin's surface potential

The zeta potential of the acidic mucin surface is analyzed by depositing a mucin monolayer onto a PCU foil. As reported in Fig.4 the pristine mucin coating on the surface of the PCU foils causes an increase of the surface potential of approximately 20 mV which confirms presence of surface bound mucins on the PCU foil.

How the contamination with charged NPs affects the surface potential of such coating was the next question. Regarding the negatively charged NPs, strong repulsion caused by the mucin's surface potential could be expected. Nevertheless, as it has just been discussed, the net surface charge reflects the overall average of the charges carried by the protein backbone. Still, positive domains in the terminal regions of the mucin molecule could locally attract the negative NPs. Moreover, in the acidic conditions, hydrophobic domains of mucin are exposed, potentially causing hydrophobic interactions with the NPs[22]These observations could justify the data shown in Fig.4: indeed, after incubation with negative NPs, a shift toward more negative potential is coherent with attachment of anionic NPs. Anyways, the strong negative charge of these NPs is likely to cause only a low level of attachment to the anionic mucin surface. Indeed, this assumption is sustained by the fact that only a modest change in zeta potential is observed in contaminated mucus.

For the positive NPs, the negative net charge of the mucin coating is expected to cause a pronounced attachment of these particles. Indeed, this interaction is evidenced by a shift in the surface potential of mucin to a positive value upon contamination.

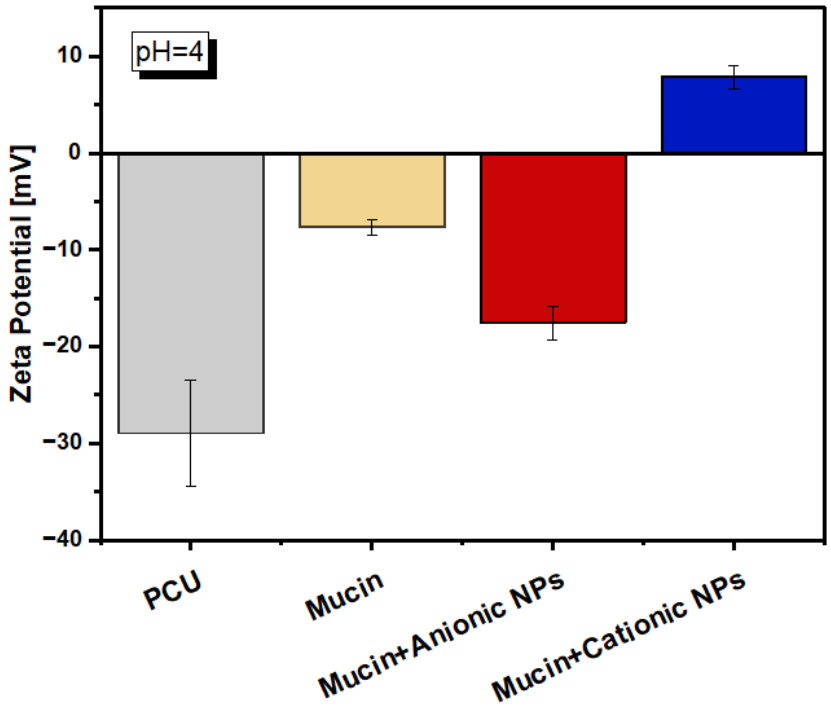

Figure 4 *Streaming potential of mucin coated foils*. Streaming potential values of uncoated PCU foil, mucin coated, and mucin coated after anionic NPs and cationic NPs contamination

n=3, error bar= STD

Notably, this result is particularly distinct from the effects of negatively charged NPs, which primarily altered the magnitude of surface charge without changing its nature. In contrast, the positive particles' contamination changed the nature of the surface, from anionic to cationic. This remarkable shift suggests that positive NPs are likely to induce more pronounced alterations in the filtration properties of mucus compared to negative NPs.

2 Microfluidic setup as a model system for mucus

In the previous section, the results were derived from experiments using two-dimensional mucin layers, focusing solely on the interactions with mucins rather than with the complete mucus layer. While such an approach provides valuable insights into the properties of mucin proteins and their interactions with nanoparticles, it does not fully capture the complexity and functionality of mucus as it exists in physiological conditions. Indeed, a mucin monolayer is essentially a single layer of mucin molecules spread out on a surface, lacking the three-dimensional network and the associated physical properties of natural mucus. In contrast, a mucus layer is a highly hydrated, gel-like matrix formed by the entanglement and cross-linking of mucin. This intricate structure contributes to the viscoelastic properties and barrier functions of mucus, affecting how particles interact with it.

To bridge this gap and better mimic the physiological environment, the subsequent phase of this study involved establishing a reconstituted mucus layer within a microfluidic device. This setup offers the advantage of creating a well-controlled interface between the mucus layer and the buffer solution, resembling the natural mucus interface found in biological systems. Studying interactions at the interface of mucus is of high importance, especially concerning nanoplastics, which are emerging as significant environmental contaminants with potential health implications. The mucus layer serves as the first line of defense in the gastrointestinal tract, trapping and regulating the passage of nutrients, drugs and pathogens. Understanding how nanoplastics interact with, adhere to, or penetrate the mucus barrier is essential for assessing their bioavailability, potential toxicity, and overall impact on human health. These interactions can influence the extent to which nanoplastics are absorbed into underlying tissues, potentially leading to adverse biological effects.

By focusing on a reconstituted mucus model within a microfluidic device, this study aims to capture the complex interactions at the mucus interface under conditions that mimic those in the human body. This approach not only enhances the relevance of the findings but also contributes to a more comprehensive understanding of the effects of NPs contamination on the mucus barrier function

2.1 Establishing a reconstituted mucus layer in a microfluidic device

Since mucins are responsible for the viscoelastic properties of this barrier, their purification and dissolution at a ratio of 2% (w/v) allows, inside the microfluidic chip, the formation of a reconstituted mucus gel column that, in terms of filtration behavior, resembles the native mucus characteristics. [20], [21]. This concentration resembles the physiologically occurring mucin concentration in the gastrointestinal tract [63] . To resemble the acidity of the gastric environment, the value of pH 4.0 is being used for all the solutions that would be used in the microfluidic chip. Even though this pH level does not exactly resemble the pH level of the gastric juices found in the stomach, which is usually around pH 2.0 it is still of physiological relevance. In fact, through the mucal layer in the stomach has a gradient of hydrochloric acid that causes the acidity to range from pH 2.0 at the superficial mucosal layer to pH 7.0 at deep mucosal layers[64]. In the body, the presence of this gradient assures survival of the cell population of the gastric lumen, that would otherwise perish from the strong acidity of the stomach's environment.

Moreover, experimental findings shows that MUC5AC mucin solutions at a concentration of 2 % (w/v) –as used for the microfluidic experiments in this study– do form a viscoelastic gel at pH of 4.0 or lower.[22]

Since the mucin type used in this study, MUC5AC, is known to undergo acidic gelation (Materials, Chapter 1.1.1), rheological measurements at acidic pH should show the presence of an elastic modulus that exceeds the viscous modulus.

Indeed, the data from rheological measurements represented in Fig. 5 shows that the mucin solution is behaving, at least partially, like a viscoelastic gel at pH 4, as indicated by the dominance of the elastic modulus *G'*.

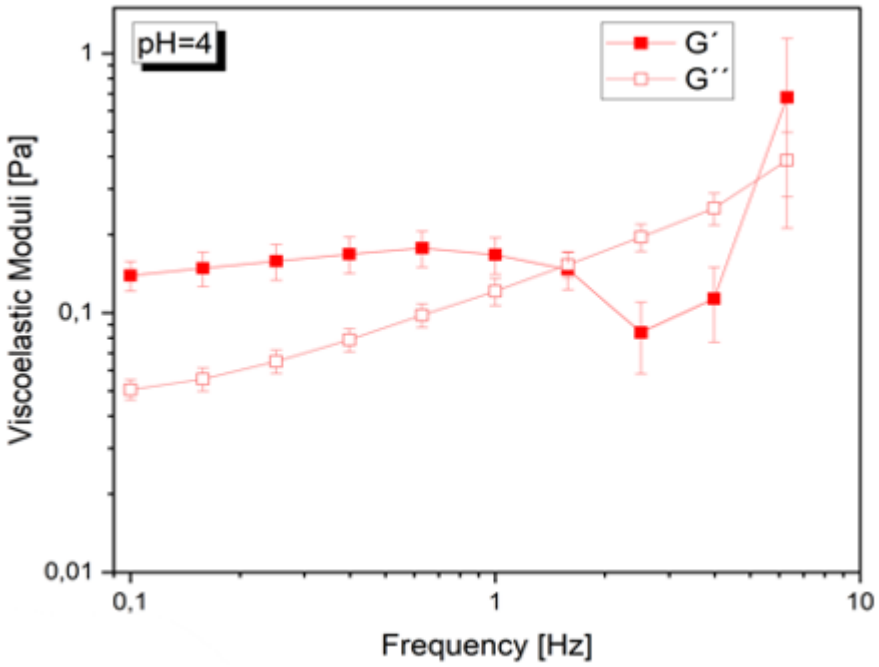

igure 5 *Frequency sweep test of MUC5AC.* Plot showing the partial predominance of the elastic modulus over the viscous modulus. The acidic solution is behaving like a partially formed viscoelastic gel.

n=3, error bar= STD

These observations indicate that, in the microfluidic setup employed in this study, the incubation with acidic buffer is capable of effectively inducing the gelation of the mucin solution utilized here. Indeed, during the incubation time the buffer that diffuses through the mucin column would gradually lower the pH around the mucin proteins, inevitably inducing the formation of a hydrogel network, and therefore the establishment of a defined sol-gel interface.

In this configuration it is then possible to investigate the interaction occurring at that interface, i.e. when nanoplastic models are contaminating the reconstituted mucus surface.

2.2 Nanoplastics accumulate at the mucus interface

Having successfully established a stable interface, the first investigation aimed at observing and understanding the interaction of nanoplastics at the mucin gel interface.

Studies have reported that polystyrene particles up to 500 nm in diameter are capable of diffusing through a mucin hydrogel[65], [66], [67] . There, the polystyrene particles that were tested had a surface coating of polyethylene glycol (PEG), a synthetic polymer known to reduce surface interactions with biological tissues, conferring antifouling properties to the surface to which it is grafted[68]. By PEGylating the particles, interactions with the mucins are hindered. As a result, the diffusion of these particles through the mucus is primarily regulated by geometrical hindrance rather than other chemical interactions. This suggests that the mesh size of the mucus is larger or at least comparable to the dimensions of the tested particles, allowing them to traverse the network with limited obstructions.

A qualitative observation (Fig 6) of the reconstituted mucus interface incubated with plastic NPs reveal that, after the incubation time, the particles do not effectively penetrate the mucus hydrogel but rather tend to adhere to its surface.

This suggests that the electrostatic attraction between the charged particles and the mucin network is strong enough to prevent their diffusion through the mucus.

These observations further support the hypothesis that polystyrene nanoplastics attach to mucus, leading to their accumulation at the surface rather than allowing for effective diffusion into the bulk of the hydrogel.

The accumulation of nanoplastics at the surface of the mucus layer might have significant implications for understanding their potential impact on biological systems. The fact that these particles accumulate at the mucus interface rather than penetrating suggests that they could potentially alter the uptake of drugs and nutrients or increase the local concentration of pollutants and toxins.

When considering particles that expose surface charges, such as those used in this study, it is reasonable to expect electrostatic interactions with the charged domains

of mucins. Indeed, mucins contain both positively and negatively charged regions, which could potentially attract or repel charged nanoparticles, thereby affecting their mobility through the mucus.[35] he polystyrene nanoplastics used here have a diameter of 300 nm, meaning that geometrical hindrance does not strongly influence their interaction with the mucus, since its mesh size should not notably hinder their diffusion. Therefore, it is logical to assume that the interactions of these particles with the mucus are primarily driven by electrostatic forces.

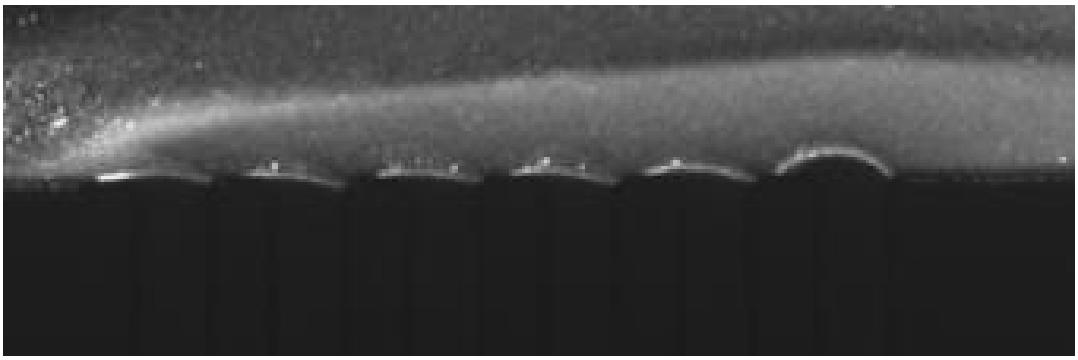

(a)

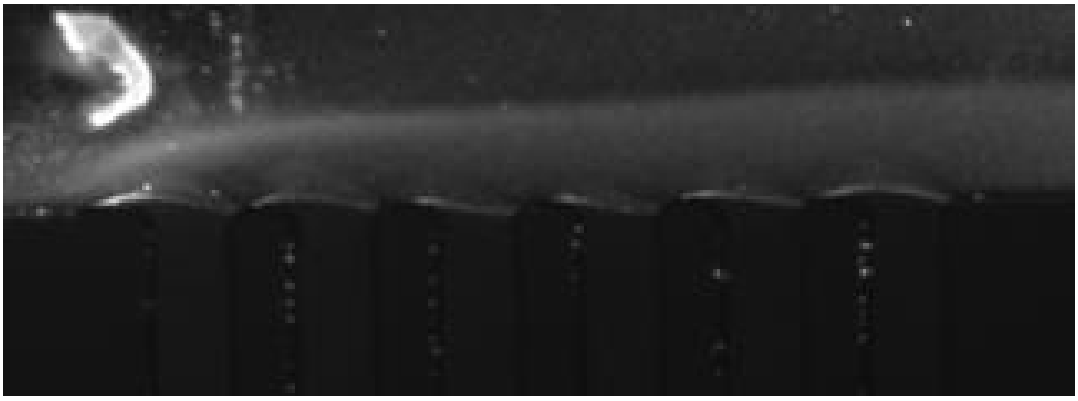

(b)

Figure 6 *Fluorescence of NPs at the reconstituted mucus interface*. Detail of the microfluidic setup showing the reconstituted mucus interface after 30 minutes of incubation and subsequent flushing out of cationic NPs (4.a) and anionic NPs (4.b) contamination. The fluorescence at the interface of the mucin layer (the 6 brighter lines) show accumulation and immobilization of both NPs variants.

3 Molecular penetration assay

3.1 Nanoplastics contaminations affect accumulation of dextrans at the mucus interface

Beyond its protective functions against mechanical, chemical, and biological threats, the mucus layer serves as a selective barrier regulating the diffusion of ions and molecules, including nutrients, drugs, and chemical pollutants[16], [69], [70]. This selective permeability is largely governed by electrostatic interactions between the mucin network and charged molecules[20]. Consequently, both the overall surface potential of mucin gels and the specific charge distributions along the mucin backbones are pivotal in controlling the translocation of biologically relevant molecules.

The molecular penetration tests used in this study employes charged dextrans to investigate the effects of nanoplastics contaminations on their ability to diffuse through the reconstituted mucus.

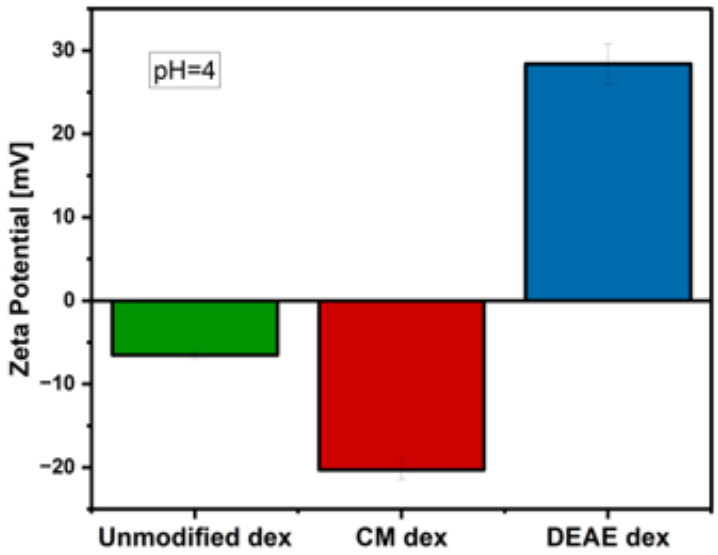

Figure 7 *Zeta potential of dextrans*. The plot shows the charge of the three dextran variants. Unmodified dextrans have very low charge, especially compared to the DEAE and CM variants.

Particular attention is given to the interactions occurring at the gel-liquid interface established in the microfluidic setup. Indeed, previous studies on pristine hydrogels [20], [21] report that while traversing a mucin gel, charged dextrans are subjected to both diffusion and a partitioning effect. Those studies found that electrostatic interactions cause the charged molecules to continuously bind and detach from the charged sites on the mucins' backbone, causing an overall reduction in the diffusing speed. This effect results in an observable accumulation of those charged molecules at the interface Indeed, the observable fluorescence peaks at the interface of uncontaminated mucus found in this study (Fig 8) points at this direction Cationic and anionic dextrans do show a certain degree of accumulation at the interface, indicated by the presence of peaks of fluorescence at the interface region. As assessed by Marczynski *et al*.[20] positive dextrans should accumulate more at the interface than negatively charged dextrans causing a higher fluorescence peaks at the mucin gel interface.

This effect is due to the relative abundance of negatively charged moieties in the mucin molecule compared the positive ones. Surprisingly, contrary to the findings by Marczynski *et al.[20], [21]* in this study, the accumulation peaks for both cationic and anionic dextrans are comparable. This result, however, is consistently observed over al large number of replicate measurements (n=25) and can most likely be attributed to the biological variation of the purified mucins used in this study compared to those used in the study by Marczynski *et al*.[20], [21] It is assumed that the mucin batch selected for these experiments presents a comparable ratio of positive and negative domains, which would explain the similar behavior observed for positive and negative dextrans. This notion is supported by the relatively modest negative surface potential found for pristine mucin coatings (see Fig. 4).

Since the previous experiments of this study pointed at the fact that NPs attach to the mucus surface modifying its surface potential, it is likely that this contamination modifies the ability of dextrans to cross the surface. Several factors such as the modification of the surface potential, the NPs occupying electrostatic binding sites or the direct interaction between the dextrans and the NPs themselves, might interfere with dextrans capacity to enter and diffuse through the mucus model employed here.

When comparing the molecular penetration behavior in pristine and contaminated models, a general look on the data shown in Fig. 8 suggests that the impact of positive NPs contamination is more pronounced in respect to the negative NPs (Fig. 9). This effect is in line with the results discussed in the previous chapter, discussing that the negative NPs contamination primarily affects the magnitude of the surface charge whereas the positive NPs change the overall charge of the mucus surface from anionic to cationic. As expected, this more accentuated modification of the surface potential resulted in a higher impact on the interactions of the dextrans at the interface. Additionally, it is likely that NPs themselves are interacting with the dextrans, influencing their attraction or repulsion from the surface. Hence, the smaller molecular penetration differences between the contaminated and the pristine groups shown in Fig.9 are coherent with the assumption that negative NPs cause only a weak contamination of the mucosal interface because they attach less to the mucus surface, *i.e.,* due to electrostatic from the anionic mucin interface.

Cationic NPs contamination

Regarding cationic NPs contamination, a high fluorescence peak for anionic dextrans' is observed at the interface, which indicates enhanced accumulation of these dextrans at the interface compared totheir behavior in the uncontaminated mucus. In the presence of cationic contaminations of the interface it seems that these dextrans are more strongly attracted to the mucus surface and then immobilized by the positive binding sites on the NPs surfaces.

Carboxylated dextrans

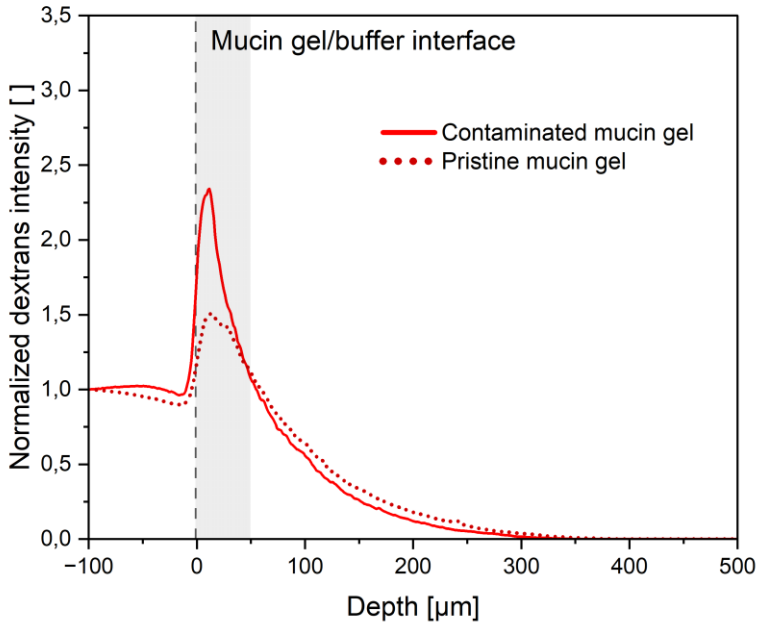

(a)

Aminated dextrans

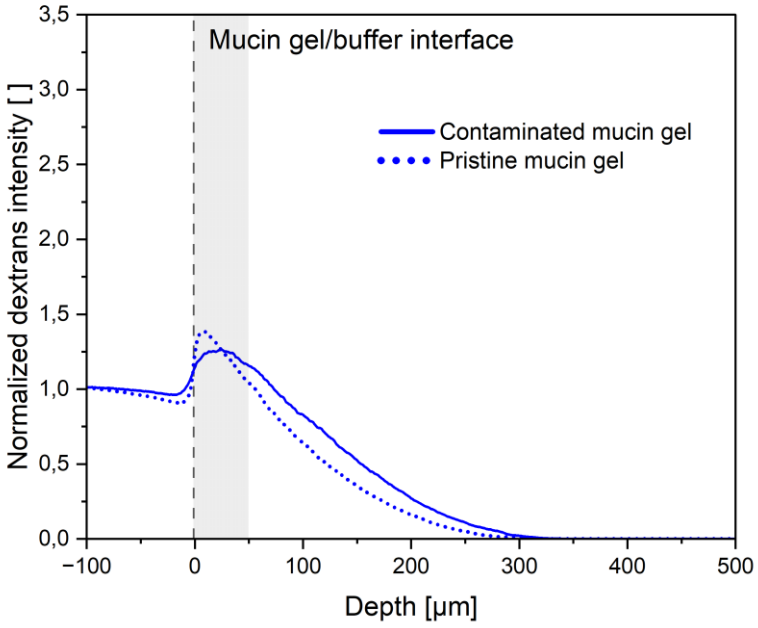

(b)

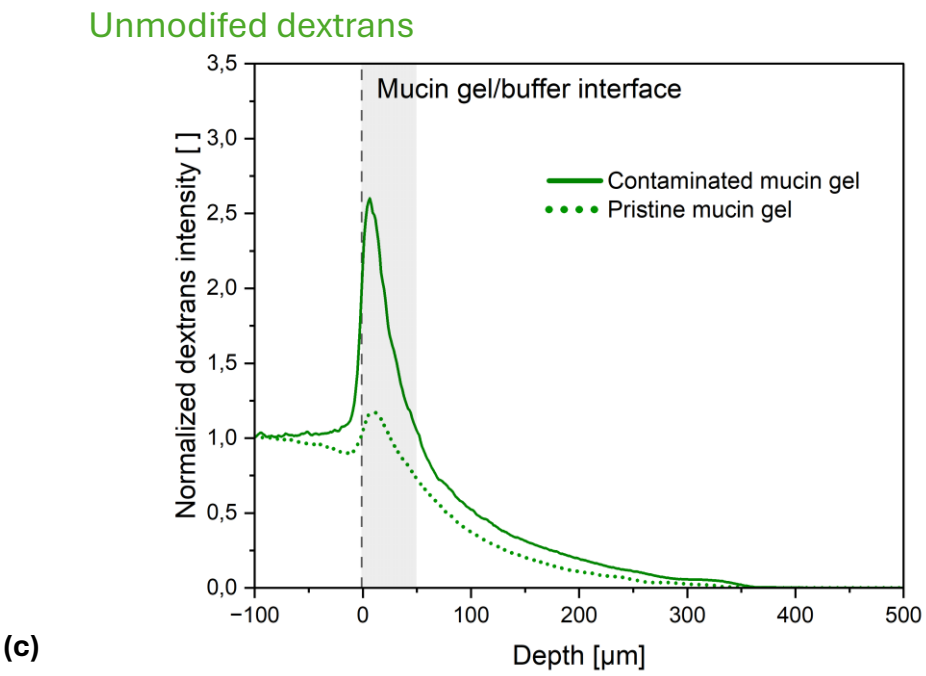

Figure 8 *Cationic contamination: molecular penetration assay.* Plots of fluorescence intensity of carboxylated (a), aminated (b) and unmodified (c) dextrans diffusing throug uncontaminated (dotted lined) and cationic NPs-contaminated mucin gel. The horizontal axis is graded so that the positive values indicate the dept inside the mucin channel while negative values indicate the buffer channel.

In contrast, when the dextrans are positively charged, a clear drop of the accumulation at the surface is observed. In addition, these cationic dextrans also appear to diffuse more rapidly than in pristine mucus, as observable by the higher fluorescence in the depth of the channel. This effect might derive from the NPs occupying the anionic binding sites on the mucins' backbone, resulting in less electrostatic interactions of the cationic dextrans at the entrance of the mucus channel. Thus, the positive dextrans would be less slowed down by those electrostatic traps, resulting in a more pronounced diffusion through the mucin gel Indeed, a similar effect has been observed for mucin gels contained with positively charged black carbon[21].

Regarding the unmodified dextrans, very low accumulation at the interface was expected. Indeed, it was reasonable to expect that their mild negative charge (see

Fig. 7) would result int less pronounced portioning effect at the effect, when compared to the behavior of the strongly anionic carboxylated dextrans. In fact, it was assumed that for dextrans with similar chemical structure and size it is their charge the main parameter governing their accumulation on the surface. This should have resulted, both in the pristine and contaminated mucus setups, in a lower magnitude of the unmodified dextrans' fluorescence signal at the interface. Indeed, the data in Fig 8.c shows low accumulation in that region for the control group. Instead, unexpectedly, when the unmodified dextrans are exposed to interfacial microplastic contaminations, a fluorescence peak higher than the one observed for the carboxylated dextrans was registered. Thus, this observation challenges the assumption that, when NPs are contaminating the mucus' surface, electrostatic interactions are the primary driving force governing dextrans' accumulation. Indeed, when the mucus surface potential is turned to positive after cationic NPs contamination, electrostatic interactions hardly justify the fact that dextrans with a less negative charge tend to accumulate more than dextrans with a stronger negative charge. This surprising effect requires further attention and will, therefore, be discussed in detail further below.

Anionic NPs contamination

The presence of anionic NPs at the interface alter the penetration behavior of carboxylated dextrans, leading to reduced accumulation at the interface. In uncontaminated mucus, positive domains on mucin backbones acted as electrostatic traps, causing carboxylated dextrans to slow down and accumulate at the interface. However, in this contaminated system, these positive sites are likely shielded by the negative charges of the NPs, resulting in decreased dextran accumulation.

Carboxylated dextrans

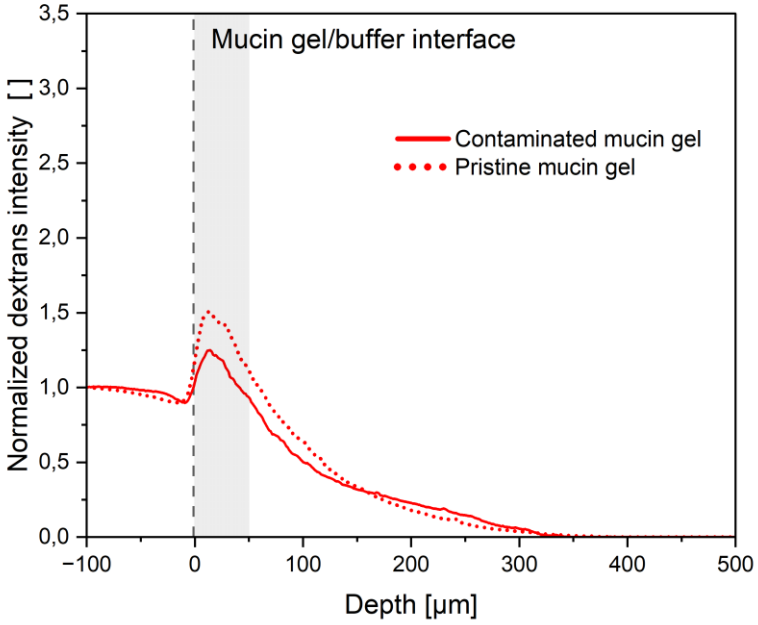

(a)

Aminated dextrans

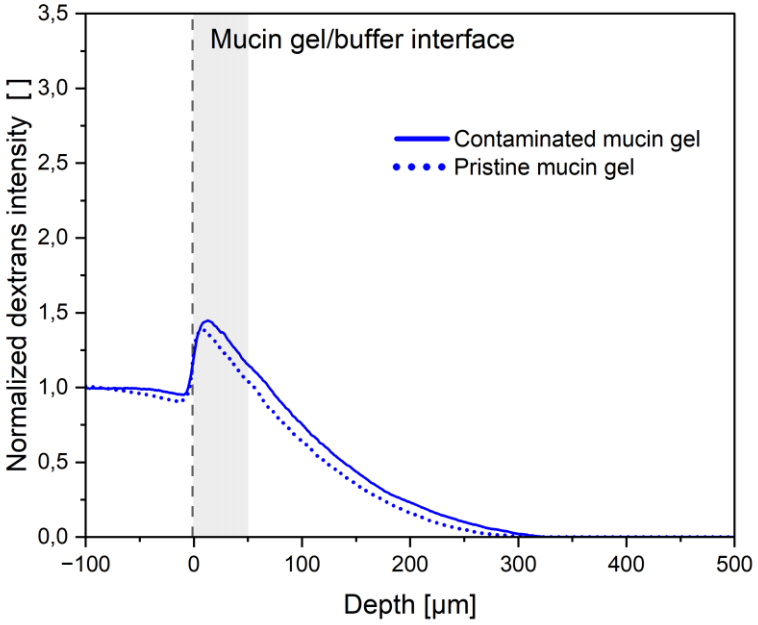

(b)

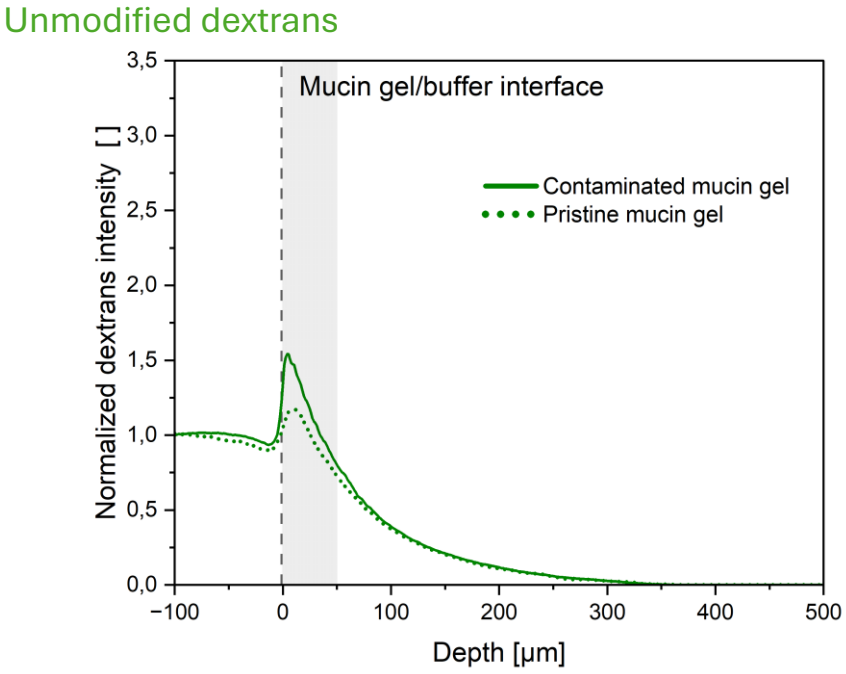

(c)

Figure 9 *Molecular penetration assay.* Plot of the fluorescence intensity of carboxylated (a), aminated (b) and unmodified (c) dextrans diffusing through uncontaminated (dotted lined) and anionic NPs-contaminated mucin gel. The horizontal axis is graded so that the positive values indicate the dept inside the mucin channel, while negative values indicate the buffer channel.

Moreover, the observed reduction , in respect to control, of fluorescence within the deeper region of the mucin gel is not surprising. Indeed, the contaminated mucus exhibits a more negative surface potential compared to the pristine system, suggesting that the carboxilate dextrans encounter increased repulsion when approaching the mucus surface. Hence, less dextrans enter the mucin gel, which may explain the reduced fluorescent signal at higher penetration depths.

This shift in surface potential also influenced the diffusion of DEAE dextrans. Although the differences from the control group are very small, there is a noticeable increase in fluorescence at higher depth in the reconstituted mucus column. This increase aligns with the enhanced electrostatic attraction experienced by the dextrans as they approach the more negatively charged contaminated surface.

Again, unmodified dextrans were expected to behave similarly to the CM ones. Instead, for this type of contamination, the unmodified dextrans showed an opposite behavior, as characterized by the increase of their accumulation at the surface. From this result, it is clear that electrostatic interactions do not explain their behavior: This points at the fact that another type of mechanism is causing their accumulation on the contaminated surface of mucus.

4 Investigating dextrans-nanoplastics interactions

4.1 Unmodified dextrans attach to nanoplastics

The fluorescence peaks at the interface given by unmodified dextrans suggested that they are accumulating in that region. Since this effect is present for both cationic and anionic NP contaminations, but is absent for a non-contaminated mucin interface, it is hypothesized that the fluorescence signal was generated from dextrans that attached to the NPs. This behavior is somewhat surprising, because the zeta potential of the unmodified dextrans is close to neutral. Hence, there is no electrostatic driving force that may govern the dextran NP interaction.

If the dextrans, indeed, attach to the NPs, it is expected that the dextrans that attach to the NPs surface would substitute the ion layer that surround them. Such a dextran coating should shield the zeta potential of the NPs. Indeed, confirming these expectations, the ELS measurement shows (Fig 10) a dramatic drop of the surface potential of cationic NPs after they were incubated with the unmodified-dextrans.

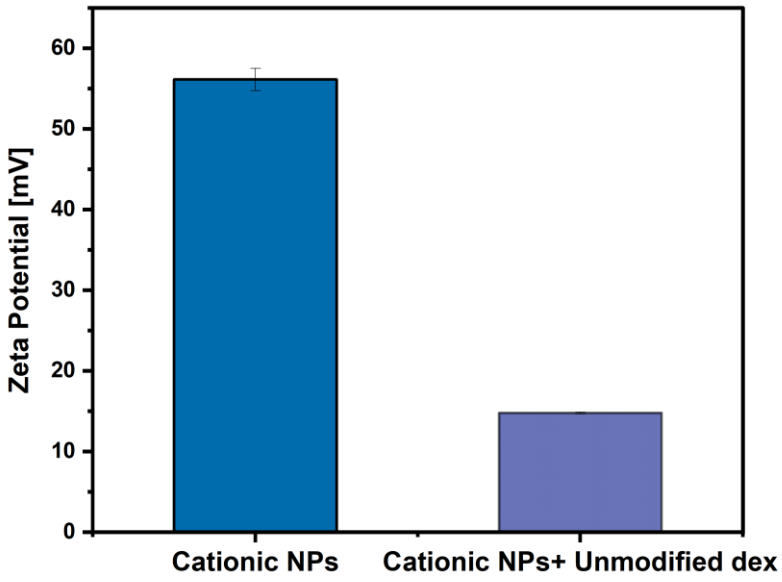

Fig 10 *Zeta potential of dextran coated NPs.* The plot shows the drop of the surface potential of cationic NPs after the incubation with an unmodified dextran solution.

Unfortunately, a similar evaluation of the zeta potential of the anionic NPs is not possible, because they show excessive aggregation when incubated with the unmodified dextrans. This aggregation of the NPs might be an indication of the decrease of their surface charge, since the loss of electrostatic repulsion could cause the aggregation of these suspended particles.

The results obtained for the cationic NPs sustain the hypothesis that the accumulation of unmodified dextrans at the mucus interface is caused by their attachment to the NPs, rather than their interaction with the charged domains on the mucin fibers that compose the hydrogel. Since these accumulation peaks were observed for both the anionic and cationic NPs contaminations, it is plausible that the dextrans-NPs interaction is not only driven by electrostatics forces. The possible nature of that interaction will be discussed in the next chapter.

4.2 Hydrophobic interactions contribute to dextrans' attachment to nanoparticles

To better understand the nature of the interactions occurring between the dextrans and the polystyrene NPs, a closer look to their chemistry is needed.

Regarding the NPs, the polymer of which they are composed, polystyrene, is inherently hydrophobic[71]. Its nature is due to its chemical structure, consisting of nonpolar aromatic rings and hydrocarbon chains (Fig. 11). The functionalization of these particles' surface with hydrophilic amino and carboxylates groups, which was necessaire to obtain oppositely charged particles, is likely to reduce the hydrophobicity of the NPs surface. Nevertheless, it is reasonable that, at least to some extent, these particles maintain their hydrophobic nature.

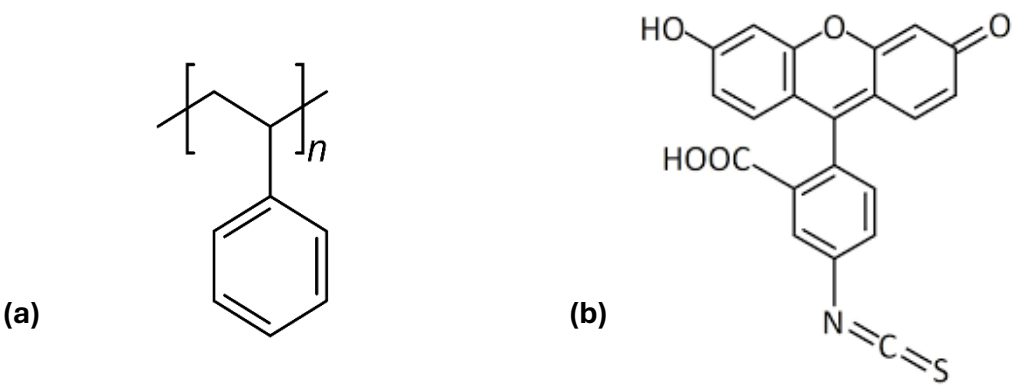

Fig 11 *Chemical structure of polystyrene and FITC.* Benzenic rings are present in both the styrene monomer (a) and FITC labeling molecule (b)

On the other hand, the three dextran variants are labeled by grafting FITC along their polysaccharidic chains. The presence of this notably hydrophobic [72] molecule is likely to decrease the inherent hydrophilic nature of the dextrans and may locally

engage in hydrophobic interactions. This effect may be pronounced for unmodified FITC-labelled dextrans due to the lack of the hydrophilic amino and carboxylates groups respectively.

By comparing the structure of the styrene monomer with the FITC molecule, it is plausible that hydrophobic interactions occur between their benzenic rings, causing attraction between the labeled dextrans and the NPs (see Fig. 10) Nevertheless, it is plausible that, when strongly charged dextrans approach the NPs, electrostatic interactions prevail on the hydrophobic ones. Indeed, as an example, the negatively charged CM-dextrans show an overall repulsion when anionic NPs are exposed on the mucus-model surface. Instead, as suggested in both the molecular penetration and the ζ-potential shielding experiments, when the dextrans expose very low charge the hydrophobic interactions may prevail, resulting in attraction towards both anionic and cationic NPs. The nature of the dextran-NP interaction may be determined by attempting to suppress the dextran attachment to the NP surface using different salts.

Chaotropic agents hinder hydrophobic interactions, while a non-chaotropic salt such as sodium chloride only hinders electrostatic interactions through Debye screening[73].

Indeed, when incubating unmodified dextrans with amine modified NPs immobilized on the surface of a well plate, the presence chaotropic salts during the incubation process result in a significant reduction (Fig. 12) of the amount of unmodified-dextrans that attach to the cationic NPs compared to a control group without additional salts. However, due to the slight negative charge of the unmodified dextrans, it is expected that also electrostatic forces contribute to the attachment of the dextrans to the NPs. In line with this expectation, also sodium chloride, a non-chaotropic salt, appears to diminish their attachment. Yet, in this last case, the differences from the control group are statically not significant, indicating that the attachment of the unmodified dextrans to the NPs is mainly driven by hydrophobic interactions.

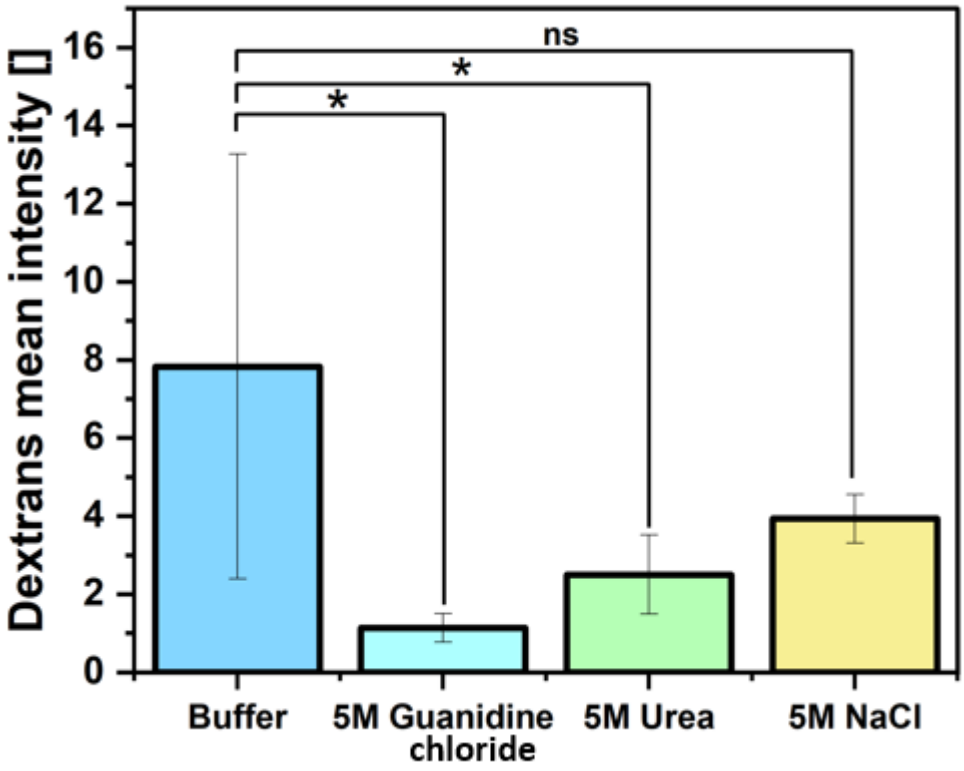

Fig 12 *Dextrans attachment fluorescence essay.* The plot shows the differences in attachment of unmodified dextrans to cationic particles when hydrophobic interactions are shielded with chaotropic agents (guanidine chloride and urea). Sodium chloride is used as a control to shield electrostatic interaction.
n=6, error bar=STD, star indicates statistical difference at $p < 0.05$

Conclusions and Outlook

This study provides elucidates the complex interactions between charged nanoplastics and the mucus barrier, emphasizing the multifaceted mechanisms by which nanoplastic contamination can alter mucosal properties. These findings are relevant to evaluate the impact of microplastics on human health. The findings of this study demonstrate that nanoplastics, regardless of their surface charge, accumulate at the mucus interface, but the nature and extent of their interactions with mucin networks differ based on their surface charge and the physicochemical properties of both the nanoparticles and the mucus.

Cationic nanoparticles appear to exhibit strong electrostatic attraction to the negatively charged domains of mucins, leading to a substantial alteration in the surface potential of the mucus layer. This interaction not only changes the net charge of the mucus surface from negative to positive but also affects its barrier function by modifying the permeability to charged molecules. The attachment of cationic nanoparticles suggests that they can significantly disrupt the selective permeability of mucus, potentially compromising its protective functions against pathogens and toxins.

Anionic nanoparticles, while expected to interact minimally due to the predominantly negative charge of mucins, still demonstrate adhesion to the mucus surface. This behavior is an indication of the fact that the mucin network contains positively charged regions capable of interacting with negatively charged nanoparticles. Although the shift in surface potential is less dramatic than with cationic nanoparticles, the accumulation of anionic nanoparticles still contributes to alterations in mucus barrier properties.

Unexpectedly, unmodified (neutral) dextrans showed significant accumulation at the mucus interface in the presence of both cationic and anionic nanoparticles. This observation could not be fully explained by electrostatic interactions alone, leading

to the consideration of hydrophobic interactions. The hydrophobic nature of polystyrene nanoparticles and the hydrophobic labeling of dextrans with fluorescein isothiocyanate most likely contribute to these interactions. This finding highlights the importance of considering non-electrostatic forces in understanding the barrier properties of contaminated mucus.

The study suggests that the interactions between nanoplastics and mucus are governed by a combination of electrostatic and hydrophobic effects. These interactions can lead to the accumulation of nanoplastics at the mucus interface, potentially disrupting the barrier function and influencing the uptake and transport of nutrients, drugs, and harmful molecules. Such alterations in mucus permeability and surface properties have significant implications for human health, particularly concerning the potential for nanoplastics to facilitate the entry of harmful substances or interfere with normal physiological processes. Moreover, the findings suggest that nanoplastic contamination can modulate the mucus barrier's selective permeability, which could affect drug delivery systems designed to traverse the mucus layer. The altered interactions between the mucus and various molecules due to nanoplastic accumulation may impact the efficacy of therapeutics and the bioavailability of orally administered drugs.

Overall, this study contributes to a deeper understanding of how nanoplastics interact with mucosal barriers, emphasizing the need for comprehensive evaluations of the risks associated with nanoplastic exposure. It highlights the importance of considering both the physicochemical properties of nanoplastics and the dynamic nature of biological barriers in assessing the potential health implications of environmental contaminants.

In the future, incorporating more complex and physiologically relevant mucus models will enhance the applicability of the results. This includes developing models that account for the dynamic nature of mucus turnover, the presence of other mucus components such as lipids and proteins, and interactions with living epithelial cells and the microbiome. Such advanced models would provide a more

comprehensive understanding of how nanoplastics affect mucus barrier function in vivo and could reveal additional mechanisms of interaction or disruption. Long-term exposure studies are also critical to assess the cumulative effects of chronic nanoplastic exposure on mucus barrier integrity and function. Investigating potential structural changes to mucins and alterations in mucus production and secretion, will provide valuable insights into the health risks associated with sustained exposure to nanoplastics. Lastly, exploring the implications for drug delivery is another important future investigation. Since the mucus barrier plays a pivotal role in drug absorption and bioavailability, understanding how nanoplastic contamination may alter mucus permeability could lead to the design of more effective drug delivery systems.

List of figures

Bibliography

[1] J. P. G. L. Frias and R. Nash, ‘Microplastics: Finding a consensus on the definition’, *Mar Pollut Bull*, vol. 138, pp. 145–147, Jan. 2019, doi: 10.1016/j.marpolbul.2018.11.022.

[2] D. K. A. Barnes, F. Galgani, R. C. Thompson, and M. Barlaz, ‘Accumulation and fragmentation of plastic debris in global environments’, *Philosophical Transactions of the Royal Society B: Biological Sciences*, vol. 364, no. 1526, pp. 1985–1998, Jul. 2009, doi: 10.1098/rstb.2008.0205.

[3] N. B. Hartmann *et al.*, ‘Are We Speaking the Same Language? Recommendations for a Definition and Categorization Framework for Plastic Debris’, *Environ Sci Technol*, vol. 53, no. 3, pp. 1039–1047, Feb. 2019, doi: 10.1021/acs.est.8b05297.

[4] L. M. Hernandez, N. Yousefi, and N. Tufenkji, ‘Are There Nanoplastics in Your Personal Care Products?’, *Environ Sci Technol Lett*, vol. 4, no. 7, pp. 280–285, Jul. 2017, doi: 10.1021/acs.estlett.7b00187.

[5] A. Banica, R. Bucur, I. Dulama, I. Bucurică, R.-M. Ştirbescu, and C. Radulescu, ‘ASSESSMENT OF MICROPLASTICS IN PERSONAL CARE PRODUCTS BY MICROSCOPIC METHODS AND VIBRATIONAL SPECTROSCOPY’, *Scientific Study & Research: Chemistry & Chemical Engineering, Biotechnology, Food Industry*, vol. 24, pp. 155–171, Dec. 2023.

[6] M. Geetha, I. M. Sasidharan Pillai, and P. Krishnamoorthy Lakshmi, ‘Photocatalytic Degradation of Microplastics: Mechanism, Recent Developments, and Associated Threats’, 2024, pp. 65–88. doi: 10.1021/bk-2024-1489.ch004.

[7] A. ter Halle *et al.*, ‘Understanding the Fragmentation Pattern of Marine Plastic Debris’, *Environ Sci Technol*, vol. 50, no. 11, pp. 5668–5675, Jun. 2016, doi: 10.1021/acs.est.6b00594.

[8] L. G. A. Barboza, A. Dick Vethaak, B. R. B. O. Lavorante, A.-K. Lundebye, and L. Guilhermino, ‘Marine microplastic debris: An emerging issue for food

security, food safety and human health', *Mar Pollut Bull*, vol. 133, pp. 336–348, Aug. 2018, doi: 10.1016/j.marpolbul.2018.05.047.

[9] 'https://www.who.int/publications/i/item/9789241516198'.

[10] J.-S. Kim, H.-J. Lee, S.-K. Kim, and H.-J. Kim, 'Global Pattern of Microplastics (MPs) in Commercial Food-Grade Salts: Sea Salt as an Indicator of Seawater MP Pollution', *Environ Sci Technol*, vol. 52, no. 21, pp. 12819–12828, Nov. 2018, doi: 10.1021/acs.est.8b04180.

[11] M. C. Rillig and A. Lehmann, 'Microplastic in terrestrial ecosystems', *Science (1979)*, vol. 368, no. 6498, pp. 1430–1431, Jun. 2020, doi: 10.1126/science.abb5979.

[12] R. Bansil and B. S. Turner, 'The biology of mucus: Composition, synthesis and organization', Jan. 15, 2018, *Elsevier B.V.* doi: 10.1016/j.addr.2017.09.023.

[13] J. Traulsen, C. Zagami, A. A. Daddi, and F. Boccellato, 'Molecular modelling of the gastric barrier response, from infection to carcinogenesis', Mar. 01, 2021, *Bailliere Tindall Ltd*. doi: 10.1016/j.bpg.2021.101737.

[14] R. A. Cone, 'Barrier properties of mucus', *Adv Drug Deliv Rev*, vol. 61, no. 2, pp. 75–85, Feb. 2009, doi: 10.1016/j.addr.2008.09.008.

[15] S. K. Lai, Y.-Y. Wang, D. Wirtz, and J. Hanes, 'Micro- and macrorheology of mucus', *Adv Drug Deliv Rev*, vol. 61, no. 2, pp. 86–100, Feb. 2009, doi: 10.1016/j.addr.2008.09.012.

[16] R. A. Cone, 'Barrier properties of mucus', *Adv Drug Deliv Rev*, vol. 61, no. 2, pp. 75–85, Feb. 2009, doi: 10.1016/j.addr.2008.09.008.

[17] J. S. Crater and R. L. Carrier, 'Barrier Properties of Gastrointestinal Mucus to Nanoparticle Transport', *Macromol Biosci*, vol. 10, no. 12, pp. 1473–1483, 2010, doi: 10.1002/mabi.201000137.

[18] S. S. Olmsted, J. L. Padgett, A. I. Yudin, K. J. Whaley, T. R. Moench, and R. A. Cone, 'Diffusion of Macromolecules and Virus-Like Particles in Human Cervical Mucus', *Biophys J*, vol. 81, no. 4, pp. 1930–1937, Oct. 2001, doi: 10.1016/S0006-3495(01)75844-4.

[19] B. S. Schuster, J. S. Suk, G. F. Woodworth, and J. Hanes, 'Nanoparticle diffusion in respiratory mucus from humans without lung disease',

Biomaterials, vol. 34, no. 13, pp. 3439–3446, Apr. 2013, doi: 10.1016/j.biomaterials.2013.01.064.

[20] M. Marczynski, B. T. Käsdorf, B. Altaner, A. Wenzler, U. Gerland, and O. Lieleg, 'Transient binding promotes molecule penetration into mucin hydrogels by enhancing molecular partitioning', *Biomater Sci*, vol. 6, no. 12, pp. 3373–3387, Dec. 2018, doi: 10.1039/c8bm00664d.

[21] M. Marczynski, T. M. Lutz, R. Schlatterer, M. Henkel, B. N. Balzer, and O. Lieleg, 'Contamination with Black Carbon Nanoparticles Alters the Selective Permeability of Mucin Hydrogels: Implications for Molecular Transport across Mucosal Barriers', *ACS Appl Nano Mater*, vol. 5, no. 11, pp. 16955–16970, Nov. 2022, doi: 10.1021/acsanm.2c03887.

[22] R. Bansil and B. S. Turner, 'Mucin structure, aggregation, physiological functions and biomedical applications', *Curr Opin Colloid Interface Sci*, vol. 11, no. 2–3, pp. 164–170, Jun. 2006, doi: 10.1016/j.cocis.2005.11.001.

[23] M. Marczynski *et al.*, 'Structural Alterations of Mucins Are Associated with Losses in Functionality', *Biomacromolecules*, vol. 22, no. 4, pp. 1600–1613, Apr. 2021, doi: 10.1021/acs.biomac.1c00073.

[24] A. P. Corfield, 'Mucins: A biologically relevant glycan barrier in mucosal protection', *Biochimica et Biophysica Acta (BBA) - General Subjects*, vol. 1850, no. 1, pp. 236–252, Jan. 2015, doi: 10.1016/j.bbagen.2014.05.003.

[25] S. Naz *et al.*, 'Unraveling the ecotoxicological effects of micro and nano-plastics on aquatic organisms and human health', *Front Environ Sci*, vol. 12, Apr. 2024, doi: 10.3389/fenvs.2024.1390510.

[26] X. Murgia, B. Loretz, O. Hartwig, M. Hittinger, and C.-M. Lehr, 'The role of mucus on drug transport and its potential to affect therapeutic outcomes', *Adv Drug Deliv Rev*, vol. 124, pp. 82–97, Jan. 2018, doi: 10.1016/j.addr.2017.10.009.

[27] D. M. Mitrano, P. Wick, and B. Nowack, 'Placing nanoplastics in the context of global plastic pollution', *Nat Nanotechnol*, vol. 16, no. 5, pp. 491–500, May 2021, doi: 10.1038/s41565-021-00888-2.

[28] S. C. Baos, D. B. Phillips, L. Wildling, T. J. McMaster, and M. Berry, 'Distribution of Sialic Acids on Mucins and Gels: A Defense Mechanism', *Biophys J*, vol. 102, no. 1, pp. 176–184, Jan. 2012, doi: 10.1016/j.bpj.2011.08.058.

[29] G. J. Strous and J. Dekker, 'Mucin-Type Glycoproteins', *Crit Rev Biochem Mol Biol*, vol. 27, no. 1–2, pp. 57–92, Jan. 1992, doi: 10.3109/10409239209082559.

[30] C. L. Hattrup and S. J. Gendler, 'Structure and Function of the Cell Surface (Tethered) Mucins', *Annu Rev Physiol*, vol. 70, no. 1, pp. 431–457, Mar. 2008, doi: 10.1146/annurev.physiol.70.113006.100659.

[31] M. E. V. Johansson, J. M. H. Larsson, and G. C. Hansson, 'The two mucus layers of colon are organized by the MUC2 mucin, whereas the outer layer is a legislator of host–microbial interactions', *Proceedings of the National Academy of Sciences*, vol. 108, no. supplement_1, pp. 4659–4665, Mar. 2011, doi: 10.1073/pnas.1006451107.

[32] L. Arike and G. C. Hansson, 'The Densely O-Glycosylated MUC2 Mucin Protects the Intestine and Provides Food for the Commensal Bacteria', *J Mol Biol*, vol. 428, no. 16, pp. 3221–3229, Aug. 2016, doi: 10.1016/j.jmb.2016.02.010.

[33] M. E. V. Johansson, H. Sjövall, and G. C. Hansson, 'The gastrointestinal mucus system in health and disease', *Nat Rev Gastroenterol Hepatol*, vol. 10, no. 6, pp. 352–361, Jun. 2013, doi: 10.1038/nrgastro.2013.35.

[34] D. J. Thornton, K. Rousseau, and M. A. McGuckin, 'Structure and Function of the Polymeric Mucins in Airways Mucus', *Annu Rev Physiol*, vol. 70, no. 1, pp. 459–486, Mar. 2008, doi: 10.1146/annurev.physiol.70.113006.100702.

[35] O. Lieleg, I. Vladescu, and K. Ribbeck, 'Characterization of particle translocation through mucin hydrogels', *Biophys J*, vol. 98, no. 9, pp. 1782–1789, May 2010, doi: 10.1016/j.bpj.2010.01.012.

[36] V. J. Schömig, B. T. Käsdorf, C. Scholz, K. Bidmon, O. Lieleg, and S. Berensmeier, 'An optimized purification process for porcine gastric mucin with preservation of its native functional properties', *RSC Adv*, vol. 6, no. 50, pp. 44932–44943, 2016, doi: 10.1039/c6ra07424c.

[37] X. Cao *et al.*, ‘pH-Dependent Conformational Change of Gastric Mucin Leads to Sol-Gel Transition’, *Biophys J*, vol. 76, no. 3, pp. 1250–1258, Mar. 1999, doi: 10.1016/S0006-3495(99)77288-7.

[38] J. Gigault *et al.*, ‘Current opinion: What is a nanoplastic?’, *Environmental Pollution*, vol. 235, pp. 1030–1034, Apr. 2018, doi: 10.1016/j.envpol.2018.01.024.

[39] C. Yong, S. Valiyaveettil, and B. Tang, ‘Toxicity of Microplastics and Nanoplastics in Mammalian Systems’, *Int J Environ Res Public Health*, vol. 17, no. 5, p. 1509, Feb. 2020, doi: 10.3390/ijerph17051509.

[40] A. L. Andrady, ‘SOURCES, FATE AND EFFECTS OF MICROPLASTICS IN THE MARINE ENVIRONMENT: PART 2 OF A GLOBAL ASSESSMENT’. [Online]. Available: https://www.researchgate.net/publication/312577266

[41] J. H. Kwon *et al.*, ‘Microplastics in food: A review on analytical methods and challenges’, Sep. 02, 2020, *MDPI AG*. doi: 10.3390/ijerph17186710.

[42] M. B. Paul *et al.*, ‘Micro- and nanoplastics – current state of knowledge with the focus on oral uptake and toxicity’, *Nanoscale Adv*, vol. 2, no. 10, pp. 4350–4367, 2020, doi: 10.1039/D0NA00539H.

[43] A. Karami, A. Golieskardi, C. Keong Choo, V. Larat, T. S. Galloway, and B. Salamatinia, ‘The presence of microplastics in commercial salts from different countries’, *Sci Rep*, vol. 7, no. 1, p. 46173, Apr. 2017, doi: 10.1038/srep46173.

[44] L. Van Cauwenberghe and C. R. Janssen, ‘Microplastics in bivalves cultured for human consumption’, *Environmental Pollution*, vol. 193, pp. 65–70, Oct. 2014, doi: 10.1016/j.envpol.2014.06.010.

[45] Y. J. He *et al.*, ‘Migration of (non-) intentionally added substances and microplastics from microwavable plastic food containers’, *J Hazard Mater*, vol. 417, Sep. 2021, doi: 10.1016/j.jhazmat.2021.126074.

[46] D. Li *et al.*, ‘Microplastic release from the degradation of polypropylene feeding bottles during infant formula preparation’.

[47] L. M. Hernandez, E. G. Xu, H. C. E. Larsson, R. Tahara, V. B. Maisuria, and N. Tufenkji, ‘Plastic Teabags Release Billions of Microparticles and

Nanoparticles into Tea', *Environ Sci Technol*, vol. 53, no. 21, pp. 12300–12310, Nov. 2019, doi: 10.1021/acs.est.9b02540.

[48] K. Chengappa S, A. Rao, A. K S, P. S. Jodalli, and R. Shenoy Kudpi, 'Microplastic content of over-the-counter toothpastes - a systematic review', *F1000Res*, vol. 12, p. 390, Apr. 2023, doi: 10.12688/f1000research.132035.1.

[49] W. Zhang, Q. Wang, and H. Chen, 'Challenges in characterization of nanoplastics in the environment', *Front Environ Sci Eng*, vol. 16, no. 1, p. 11, Jan. 2022, doi: 10.1007/s11783-021-1445-z.

[50] G. Stojkov, Z. Niyazov, F. Picchioni, and R. K. Bose, 'Relationship between structure and rheology of hydrogels for various applications', Dec. 01, 2021, *MDPI*. doi: 10.3390/gels7040255.

[51] C. A. Rickert, B. Wittmann, R. Fromme, and O. Lieleg, 'Highly Transparent Covalent Mucin Coatings Improve the Wettability and Tribology of Hydrophobic Contact Lenses', *ACS Appl Mater Interfaces*, vol. 12, no. 25, pp. 28024–28033, Jun. 2020, doi: 10.1021/acsami.0c06847.

[52] D. C. Duffy, J. C. McDonald, O. J. A. Schueller, and G. M. Whitesides, 'Rapid prototyping of microfluidic systems in poly(dimethylsiloxane)', *Anal Chem*, vol. 70, no. 23, pp. 4974–4984, Dec. 1998, doi: 10.1021/ac980656z.

[53] J. Abenojar, I. Colera, M. A. Martínez, and F. Velasco, 'Study by XPS of an atmospheric plasma-torch treated glass: Influence on adhesion', in *Journal of Adhesion Science and Technology*, Aug. 2010, pp. 1841–1854. doi: 10.1163/016942410X507614.

[54] C. Lee, H. W. Kim, and S. Kim, 'Organic contaminants removal by oxygen ECR plasma', *Appl Surf Sci*, vol. 253, no. 7, pp. 3658–3663, Jan. 2007, doi: 10.1016/j.apsusc.2006.07.075.

[55] T. L. Abell *et al.*, 'Consensus recommendations for gastric emptying scintigraphy: A joint report of the American Neurogastroenterology and Motility Society and the Society of Nuclear Medicine', Mar. 2008. doi: 10.2967/jnmt.107.048116.

[56] D. A. Norris and P. J. Sinko, 'Effect of size, surface charge, and hydrophobicity on the translocation of polystyrene microspheres through gastrointestinal

mucin', *J Appl Polym Sci*, vol. 63, no. 11, pp. 1481–1492, Mar. 1997, doi: 10.1002/(SICI)1097-4628(19970314)63:11<1481::AID-APP10>3.0.CO;2-5.

[57] J. Y. Lock, T. L. Carlson, and R. L. Carrier, 'Mucus models to evaluate the diffusion of drugs and particles', *Adv Drug Deliv Rev*, vol. 124, pp. 34–49, Jan. 2018, doi: 10.1016/j.addr.2017.11.001.

[58] S. Sarkar, H. Diab, and J. Thompson, 'Microplastic Pollution: Chemical Characterization and Impact on Wildlife', Feb. 01, 2023, *MDPI*. doi: 10.3390/ijerph20031745.

[59] A. M. N. A. A. Rahman *et al.*, 'A review of microplastic surface interactions in water and potential capturing methods', Dec. 01, 2024, *Editorial Office of Water Science and Engineering*. doi: 10.1016/j.wse.2023.11.008.

[60] C. Campanale, C. Massarelli, I. Savino, V. Locaputo, and V. F. Uricchio, 'A detailed review study on potential effects of microplastics and additives of concern on human health', Feb. 02, 2020, *MDPI AG*. doi: 10.3390/ijerph17041212.

[61] S. Sarkar, H. Diab, and J. Thompson, 'Microplastic Pollution: Chemical Characterization and Impact on Wildlife', Feb. 01, 2023, *MDPI*. doi: 10.3390/ijerph20031745.

[62] N. Rafa *et al.*, 'Microplastics as carriers of toxic pollutants: Source, transport, and toxicological effects', *Environmental Pollution*, vol. 343, p. 123190, Feb. 2024, doi: 10.1016/j.envpol.2023.123190.

[63] C. TAYLOR, 'Two rheologically different gastric mucus secretions with different putative functions', *Biochimica et Biophysica Acta (BBA) - General Subjects*, Jul. 2004, doi: 10.1016/j.bbagen.2004.06.007.

[64] H. M. Bahari, I. N. Ross, and L. A. Turnberg, 'Demonstration of a pH gradient across the mucus layer on the surface of human gastric mucosa in vitro.', *Gut*, vol. 23, no. 6, pp. 513–516, Jun. 1982, doi: 10.1136/gut.23.6.513.

[65] K. Yoncheva, S. Gómez, M. A. Campanero, C. Gamazo, and J. M. Irache, 'Bioadhesive properties of pegylated nanoparticles', *Expert Opin Drug Deliv*, vol. 2, no. 2, pp. 205–218, Mar. 2005, doi: 10.1517/17425247.2.2.205.

[66] S. S. Olmsted, J. L. Padgett, A. I. Yudin, K. J. Whaley, T. R. Moench, and R. A. Cone, 'Diffusion of Macromolecules and Virus-Like Particles in Human

Cervical Mucus', *Biophys J*, vol. 81, no. 4, pp. 1930–1937, Oct. 2001, doi: 10.1016/S0006-3495(01)75844-4.

[67] S. K. Lai *et al.*, 'Rapid transport of large polymeric nanoparticles in fresh undiluted human mucus', *Proceedings of the National Academy of Sciences*, vol. 104, no. 5, pp. 1482–1487, Jan. 2007, doi: 10.1073/pnas.0608611104.

[68] J. S. Suk, Q. Xu, N. Kim, J. Hanes, and L. M. Ensign, 'PEGylation as a strategy for improving nanoparticle-based drug and gene delivery.', *Adv Drug Deliv Rev*, vol. 99, no. Pt A, pp. 28–51, Apr. 2016, doi: 10.1016/j.addr.2015.09.012.

[69] S. Cornick, A. Tawiah, and K. Chadee, 'Roles and regulation of the mucus barrier in the gut', *Tissue Barriers*, vol. 3, no. 1–2, p. e982426, Apr. 2015, doi: 10.4161/21688370.2014.982426.

[70] P. Paone and P. D. Cani, 'Mucus barrier, mucins and gut microbiota: The expected slimy partners?', Dec. 01, 2020, *BMJ Publishing Group*. doi: 10.1136/gutjnl-2020-322260.

[71] G. Wypych, 'PS polystyrene', in *Handbook of Polymers*, Elsevier, 2012, pp. 541–547. doi: 10.1016/B978-1-895198-47-8.50162-4.

[72] 'https://pubchem.ncbi.nlm.nih.gov/compound/Fluorescein-5-isothiocyanate'.

[73] G. Salvi, P. De Los Rios, and M. Vendruscolo, 'Effective interactions between chaotropic agents and proteins', *Proteins: Structure, Function, and Bioinformatics*, vol. 61, no. 3, pp. 492–499, Nov. 2005, doi: 10.1002/prot.20626.